

1 Long-Range Aerosol Transport and Impacts on Size-Resolved Aerosol Composition in Metro
2 Manila, Philippines

3
4 Rachel A. Braun¹, Mojtaba Azadi Aghdam¹, Paola Angela Bañaga^{2,3}, Grace Betito³, Maria
5 Obiminda Cambaliza^{2,3}, Melliza Templonuevo Cruz^{2,4}, Genevieve Rose Lorenzo², Alexander B.
6 MacDonald¹, James Bernard Simpas^{2,3}, Connor Stahl¹, Armin Sorooshian^{1,5}

7
8
9 ¹Department of Chemical and Environmental Engineering, University of Arizona, Tucson, AZ,
10 USA

11 ²Manila Observatory, Loyola Heights, Quezon City 1108, Philippines

12 ³Department of Physics, School of Science and Engineering, Ateneo de Manila University,
13 Loyola Heights, Quezon City 1108, Philippines

14 ⁴Institute of Environmental Science and Meteorology, University of the Philippines, Diliman,
15 Quezon City 1101, Philippines

16 ⁵Department of Hydrology and Atmospheric Sciences, University of Arizona, Tucson, AZ, USA

17

18 Correspondence to: Armin Sorooshian (armin@email.arizona.edu)

19 **Abstract**

20 This study analyzes long-range transport of aerosol and aerosol chemical characteristics based on
21 instances of high and low aerosol loading events determined via ground-based size-resolved
22 aerosol measurements collected at the Manila Observatory in Metro Manila, Philippines from
23 July - October 2018. Multiple data sources, including models, remote-sensing, and in situ
24 measurements, are used to analyze the impacts of long-range aerosol transport on Metro Manila
25 and the conditions at the local and synoptic scales facilitating this transport. Through the use of
26 case studies, evidence of long-range transport of biomass burning aerosol and continental
27 emissions is identified in Metro Manila. Long-range transport of biomass burning aerosol from
28 the Maritime Continent, bolstered by southwesterly flow and permitted by low rainfall, was
29 identified through model results and the presence of biomass burning tracers (e.g. K, Rb) in the
30 ground-based measurements. The impacts of emissions transported from continental East Asia
31 on the aerosol characteristics in Metro Manila are also identified; for one of the events analyzed,
32 this transport was facilitated by the nearby passage of a typhoon. Changes in the aerosol size
33 distributions, water-soluble chemical composition, and contributions of various organic aerosol
34 species to the total water-soluble organic aerosol were examined for the different cases. The
35 events impacted by biomass burning transport had the overall highest concentration of water-
36 soluble organic acids, while the events impacted by long-range transport from continental East
37 Asia, showed high percent contributions from shorter chain dicarboxylic acids (i.e. oxalate) that
38 are often representative of photochemical and aqueous processing in the atmosphere. The low
39 aerosol loading event was subject to a larger precipitation accumulation than the high aerosol
40 events, indicative of wet scavenging as an aerosol sink in the study region. This low aerosol
41 event was characterized by a larger relative contribution from supermicrometer aerosols and had
42 a higher percent contribution from longer-chain dicarboxylic acids (i.e. maleate) to the water-
43 soluble organic aerosol fraction, indicating the importance of both primary aerosol emissions and
44 local emissions.

45 **1. Introduction**

46 Better understanding of long-range transport of aerosol is critical for determining the fate
47 of atmospheric emissions and improving models of atmospheric aerosol. Nutrients (e.g. Duce et
48 al., 1991; Artaxo et al., 1994), bacteria (e.g. Bovallius et al., 1978; Maki et al., 2019), and
49 pollutants (e.g. Nordø, 1976; Lyons et al., 1978; Lindqvist et al., 1991) can be transported
50 through the atmosphere over large distances across the globe. Atmospheric aerosol can undergo
51 physiochemical changes through photochemical and aqueous-processing mechanisms such that
52 their characteristics at the emission source can be quite different from those farther downwind
53 (e.g. Yokelson et al., 2009; Akagi et al., 2012). Large uncertainties remain in atmospheric
54 aerosol models due to impacts of aqueous processing and wet scavenging on aerosol (Kristiansen
55 et al., 2016; Xu et al., 2019).

56 The plethora of both natural and anthropogenic emissions in and around the Southeast
57 (SE) Asia, the proximity of islands and continental regions in SE and East Asia, and the large,
58 growing population makes SE Asia a prime candidate for the study of long-range transport of
59 atmospheric aerosol. Moreover, the extensive cloud coverage and precipitation during certain
60 times of the year in SE Asia allow for an examination of the effects of aqueous processing and
61 wet scavenging. Characterizations of aerosol in mainland SE Asia and the Maritime Continent
62 (MC), which includes the islands south of the Philippines and north of Australia (e.g. islands part
63 of Malaysia and Indonesia), have found major emission sources to be industrial activities,
64 shipping, urban mega-cities, and biomass burning (Reid et al., 2013). In addition, natural
65 emission sources, including marine emissions, plant life, and occasionally volcanic eruptions,
66 intermingle with anthropogenic emissions. Mixing of aerosol from anthropogenic and biogenic
67 sources has been noted to be influential in the overall production of secondarily produced aerosol
68 via gas-to-particle conversion processes (Weber et al., 2007; Goldstein et al., 2009; Brito et al.,
69 2018). In addition, the mixing of marine and biomass burning emissions can produce
70 compositional changes, such as enhancements in chloride depletion (e.g. Braun et al., 2017) and
71 methanesulfonate (MSA) production (Sorooshian et al., 2015). The mechanisms governing
72 aerosol changes in mixed air masses have wide-ranging and complex impacts and require further
73 study in regions, such as SE Asia, that are impacted by multiple aerosol emission sources.

74 One major contributor to atmospheric aerosol in SE Asia and the MC that has received
75 considerable attention is biomass burning. Biomass burning in SE Asia appears to be dominated
76 by anthropogenic activities, such as peatland burning (Graf et al., 2009; Reid et al., 2013; Latif et
77 al., 2018) and rice straw open field burning (Gadde et al., 2009). However, current satellite
78 retrievals underestimate the true emissions in the region (Reid et al., 2013). Identification of
79 biomass burning emissions in the MC using satellite-based observations is difficult for numerous
80 reasons, including the characteristics of fires common to the region (e.g. low-temperature peat-
81 burning) and abundant cloud cover (Reid et al., 2012, 2013). However, the potential for long-
82 range transport of biomass burning emissions from the MC has received considerable attention
83 (Wang et al., 2013; Xian et al., 2013; Reid et al., 2016a; Atwood et al., 2017; Ge et al., 2017;
84 Song et al., 2018). In order to better understand the frequency, amount, and fate of biomass
85 burning emissions in the MC and SE Asia, both in situ measurements and modeling studies are
86 needed. Insights into the fate of biomass burning emissions in the atmosphere are crucial and
87 applicable on a global scale, especially since studies have indicated an increasing trend in
88 biomass burning worldwide (Flannigan et al., 2009, 2013).

89 As a mega-city in SE Asia, Metro Manila, Philippines (Population ~12.88 million;
90 Philippine Statistics Authority, 2015) is a prime location for the study of locally-produced urban

91 anthropogenic aerosol (Kim Oanh et al., 2006) that is mixed with biogenic, natural, and
92 anthropogenic pollutants from upwind areas. Previous research conducted at the Manila
93 Observatory (MO) in Quezon City, Metro Manila characterized PM_{2.5} (particulate matter (PM)
94 with aerodynamic diameter less than 2.5 μm) and sources of measured particles, with traffic
95 emissions being the major source at MO (Simpas et al., 2014). Interestingly, levels of measured
96 PM_{2.5} at MO showed little variance between the wet (June-October) and dry seasons (Simpas et
97 al., 2014). Additional studies have further characterized vehicular emissions by focusing on
98 black carbon (BC) particulate concentrations in sites around the Metro Manila region, including
99 near roadways (Bautista et al., 2014; Kecorius et al., 2017; Alas et al., 2018). Due to very high
100 population density in Metro Manila, it is expected that many of the urban PM sampling sites are
101 highly affected by local anthropogenic sources as opposed to long-range transport. However, the
102 proximity of the Philippines to other islands and continental Asia raises the question of the
103 relative impacts of long-range transport as opposed to local emissions on not just Metro Manila,
104 but also downwind regions.

105 Long-range transport to the Philippines varies by season since there is a strong change in
106 weather patterns throughout the year (Bagtasa et al., 2018). Another study of the aerosol over the
107 South China Sea (SCS), which is bordered to the east by the Philippines, found seasonal changes
108 in aerosol emission sources, with year-round anthropogenic pollution, smoke from the MC
109 between August – October, and dust from northern continental Asia between February – April
110 (Lin et al., 2007). The season from approximately June – September (Cayanan et al., 2011; Cruz
111 et al., 2013), referred to as the Southwest Monsoon (SWM) season, is characterized by increased
112 prevalence of southwesterly winds and precipitation. During the SWM season, biomass burning
113 is prevalent in the MC, while biomass burning is more common in continental SE Asia during
114 the winter and spring (Lin et al., 2009; Reid et al., 2013). While variability exists in the start dates
115 of the different seasons, the northeast monsoon transition generally occurs in October (Cruz et
116 al., 2013), and previous research has defined this season as occurring from October – February
117 (Bagtasa, 2011). During the northeast monsoon, aerosol influences from northern East Asia were
118 measured in the northwestern edge of the Philippines (Bagtasa et al., 2018). In addition to
119 transport of aerosol to the Philippines, the influence of emission outflows from the Philippines
120 has also been measured in the northern SCS at Dongsha Island (Chuang et al., 2013) and in
121 coastal southeast China (Zhang et al., 2012). Long-range transported aerosol in SE and East Asia
122 have various sources, and therefore, different physiochemical properties. However, the
123 prevalence of the signal of long-range transported aerosol in a highly polluted mega-city, such as
124 Metro Manila, is not well characterized.

125 As recent studies have indicated a decline in SWM rainfall in the western Philippines and
126 an increase in no-rain days during the typical SWM season (Cruz et al., 2013), the potential for
127 wet scavenging of aerosol during these time periods could be decreasing. Furthermore, decreases
128 in monsoonal rainfall in other parts of Asia, including India (Dave et al., 2017) and China (Liu et
129 al., 2019), have been linked to increases in aerosol, especially those of anthropogenic origin.
130 Reinforcing mechanisms in these interactions, such as decreased rainfall reducing wet
131 scavenging, leading to higher aerosol concentrations that in turn suppress precipitation, and the
132 corresponding climatic changes in monsoonal rain in the western Philippines underscore the need
133 to better understand the processes governing atmospheric aerosol characteristics and sources,
134 especially during the monsoonal season.

135 The present study focuses on three high aerosol loading events, contrasted with a very
136 low aerosol event, as identified by ground-based observations collected at MO from July -

137 October 2018. The objectives of the study are to (i) describe synoptic and local scale conditions
138 facilitating various transport cases, (ii) characterize aerosol physicochemical properties
139 associated with long-range transport, and (iii) identify transformational processes, especially
140 with regard to chemical composition, of aerosol during long-range transport to the highly-
141 populated Metro Manila region. The results of this work have implications for better
142 understanding of (i) the fate of biomass burning emissions in a region with prevalent wildfires
143 that are poorly characterized by remote-sensing, (ii) the impact of transformational and removal
144 mechanisms, including aqueous processing, photochemical reactions, and wet scavenging, on
145 long-range transported aerosol from multiple sources, and (iii) typical synoptic and local scale
146 behavior of aerosol in a region that is both highly populated and gaining increasing attention due
147 to campaigns such as the NASA-sponsored Clouds, Aerosols, and Monsoon Processes
148 Philippines Experiment (CAMP²Ex).

149 150 **2. Methodology**

151 **2.1 Ground-Based Observations**

152 As part of a year-long sampling campaign (CAMP²Ex weathER and CompoSition
153 Monitoring: CHECSM) at the Manila Observatory (MO; 14.64° N, 121.08° E) in Quezon City,
154 Metro Manila, Philippines, 12 sets of size-resolved aerosol were collected from July - October
155 2018 using a Micro-Orifice Uniform Deposit Impactor (MOUDI; Marple et al., 2014). Details
156 for the 12 size-resolved sets can be found in Table 1. Sample Teflon substrates (PTFE
157 membrane, 2 μm pore, 46.2 mm diameter, Whatman) were cut in half for preservation for future
158 analysis. Half-substrates were extracted in 8 mL of Milli-Q water (18.2 MΩ-cm) in sealed
159 polypropylene vials through sonication for 30 min. Aqueous extracts were subsequently analyzed
160 for ions using ion chromatography (IC; Thermo Scientific Dionex ICS-2100 system) and
161 elements using triple quadrupole inductively coupled plasma mass spectrometry (ICP-QQQ;
162 Agilent 8800 Series). The list of analyzed species and limits of detection for those species can be
163 found in Table S1, with limits of detection in the ppt range for ICP and the ppb range for IC.
164 Background concentrations were also subtracted from each sample. For each MOUDI set
165 (naming convention: MO#), the mass concentration sum of the water-soluble species was
166 calculated; using this summation, the three high aerosol loading events were identified (MO7,
167 MO12, and MO14), as well as the lowest aerosol event (MO11). The average ± standard
168 deviation of the total-water soluble species measured for the remaining 8 sets not identified in
169 the high or low categories is $6.99 \pm 2.71 \mu\text{g m}^{-3}$.

170 171 **2.2 Remote-Sensing Observations**

172 Retrievals of atmospheric profiles from the Cloud-Aerosol Lidar with Orthogonal
173 Polarization (CALIOP) onboard the Cloud-Aerosol Lidar and Infrared Pathfinder Satellite
174 Observations (CALIPSO) were taken for select satellite overpasses corresponding to MOUDI
175 sample sets of interest (Winker et al., 2009). Previous studies have examined the ability of
176 CALIOP to capture atmospheric profiles in SE Asia and the MC, with one major challenge in
177 this region being the lack of cloud-free schemes (Campbell et al., 2013; Ross et al., 2018).
178 Overpasses corresponding to the three highest aerosol events were analyzed, but no data was
179 available for the time encompassing MO11. The CALIOP Level 2 Vertical Feature Mask (VFM)
180 Version 4.20 was used to distinguish between clear air, clouds, and aerosol (Vaughan et al.,
181 2004). For figures of CALIOP VFM data in this study, data are plotted at 30 m vertical
182 resolution every 5 km along the satellite ground-track.

183
184
185
186
187
188
189
190
191
192
193
194
195
196
197
198
199
200
201
202
203
204
205
206
207
208
209
210
211
212
213
214
215
216
217
218
219
220
221
222
223
224
225
226
227
228

2.3 Models

To describe the synoptic scale conditions, data were used from the Modern-Era Retrospective analysis for Research and Applications, Version 2 (MERRA-2; Gelaro et al., 2017). Horizontal winds at 850 hPa (GMAO, 2015a) were temporally averaged over the sampling period using 3-hourly instantaneous data and subsequently spatially averaged to increase figure readability. The total cloud area fraction (GMAO, 2015b) was also temporally averaged over the sampling period using 1-hourly time-averaged MERRA-2 data.

Five-day air mass back-trajectories were calculated using the Hybrid Single Particle Lagrangian Integrated Trajectory (HYSPLIT) model from NOAA (Stein et al., 2015) and gridded meteorological data from the National Centers for Environmental Prediction/National Center for Atmospheric Research (NCEP/NCAR) reanalysis project. The model was run for back-trajectories terminating at the MOUDI inlet (~85 m above sea level) starting at the beginning of the sample set and every 6 h thereafter during each sample set, resulting in $(1 + N/6)$ trajectories for each set, where N is the total number of sampling hours. Heights above ground level for HYSPLIT back-trajectories corresponding to the three high aerosol loading events (MO7, MO12, and MO14) can be found in Figure S1. The HYSPLIT model has been used extensively in studies focused on regions across the globe to study aerosol transport (Stein et al., 2015).

Precipitation amounts were found using the Precipitation Estimation from Remotely Sensed Information using Artificial Neural Networks—Cloud Classification System (PERSIANN-CCS) dataset (Hong et al., 2004), which is available from the UC Irvine Center for Hydrometeorology and Remote Sensing (CHRS) Data Portal (<http://chrsdata.eng.uci.edu>, Nguyen et al., 2019). PERSIANN-CCS has previously been used to analyze precipitation events in the region of interest, as shown by the successful characterization of rainfall during Typhoon Haiyan over the Philippines in November 2013 (Nguyen et al., 2014). Benefits of PERSIANN-CCS include the data availability at $0.04^\circ \times 0.04^\circ$ spatial resolution, while uncertainties in the dataset arise from sources such as a lack of bias correction (Nguyen et al., 2014). Precipitation accumulated during the sample sets (Table 1) was calculated to be the average found for the region surrounding MO in the box bounded by $121.0199 - 121.0968^\circ$ E and $14.6067 - 14.6946^\circ$ N.

To further describe long-range transport activity, results from the Navy Aerosol Analysis and Prediction System (NAAPS) operational model are included for the selected study periods (Lynch et al., 2016; <https://www.nrlmry.navy.mil/aerosol/>). Global meteorological fields used in the NAAPS model are supplied by the Navy Global Environmental Model (NAVGEM; Hogan et al., 2014). The NAAPS model has previously been employed to study aerosol in the MC (e.g. Xian et al., 2013).

3. Results

3.1 Cases of Long-Range Aerosol Transport

The following sub-sections (3.1.1-3.1.4) describe the synoptic and local scale meteorological conditions governing long-range aerosol transport during the three highest aerosol events (MO7, MO12, and MO14) and, for the purposes of comparison, the lowest aerosol event (MO11). Also included are characterizations of aerosol from remote-sensing and model results. Results of size-resolved aerosol characterization at MO are discussed in Section 3.2.

229 **3.1.1 MO7 (August 14 – 16, 2018): Smoke Transport from Maritime Continent**

230 Many previous studies have focused on the prevalence of biomass burning in the MC and
231 the potential for transport of smoke towards the Philippines (Wang et al., 2013; Xian et al., 2013;
232 Reid et al., 2016a; Atwood et al., 2017; Ge et al., 2017; Song et al., 2018). Figure 1a shows the
233 average 850 hPa wind vectors and cloud fraction for the MO7 sampling period. The prevailing
234 wind direction was towards the northeast, consistent with typical SWM flow. Furthermore, areas
235 with lower cloud coverage were present to the southwest of Metro Manila. The HYSPLIT back-
236 trajectory for this sample set also shows an air mass originating around the MC to the southwest
237 of MO that is then transported over the ocean towards the Philippines (Figure 2a). As evidenced
238 by the name of the season (i.e. Southwest Monsoon), this trajectory is typical for this time of the
239 year and was the dominating trajectory pattern for the remaining eight sample sets not chosen for
240 in-depth analysis (Figure S2). Furthermore, for MO1 – MO10 (i.e. all sample sets with prevailing
241 southwesterly wind influence), MO7 had the lowest rain amount for the surrounding region,
242 followed by MO8, which had the 4th highest water-soluble aerosol concentration (Table 1). This
243 suggests that wet scavenging could have been less influential in MO7 and MO8, thereby leading
244 to an increase in the PM measured. Three CALIPSO overpasses near MO occurred during the
245 MO7 sample set and one occurred during the nighttime after sampling ended; however, the
246 signal was largely attenuated in the lower 8 km during the daytime samples for the area
247 surrounding MO (Figure S3). In the case of the two nighttime overpasses (Figure 3), which
248 sampled to the southwest of Manila, a deep aerosol layer is observed in the VFM extending from
249 the surface to around 3 km (Figure 3). This classic case of long-range transport from the MC to
250 the Philippines during the SWM season is also clearly shown in the biomass burning smoke
251 surface concentrations from the NAAPS model (Figure 4a).

252 **3.1.2 MO11 (September 18 – 20, 2018): Lowest Aerosol Event**

253 MO11 had the lowest overall water-soluble aerosol mass concentration ($2.7 \mu\text{g m}^{-3}$),
254 which is over six times lower than the highest aerosol MOUDI set. As evidenced by both the 850
255 hPa wind vectors (Figure 1b) and the HYSPLIT back-trajectories (Figure 2b) from this set,
256 conditions are very different from the highest three aerosol events and show transport patterns
257 with flow originating over the open ocean to the east of the Philippines moving almost due west.
258 The lack of anthropogenic aerosol sources in the path of the back-trajectories could result in the
259 overall low amount of aerosol observed. This set was also characterized by high accumulated
260 rainfall amounts for the region in the path of the back-trajectories (Figure 2b) and in the area
261 surrounding MO as compared to the highest aerosol events (Table 1), increasing the possibility
262 that wet scavenging effectively removed most of the transported (and, to some extent, local)
263 aerosol. In addition, the NAAPS model showed no smoke influence from the MC and an isolated
264 anthropogenic and biogenic fine aerosol plume around Metro Manila, suggesting local sources
265 accounted for the majority of the measured aerosol (Figure 4b).

266 **3.1.3 MO12 (September 26 – 28, 2018): Impacts of Typhoon Trami**

267 Typhoon Trami (Category 5) passed to the northeast of the island of Luzon in the
268 Philippines during MO12 (Figure 1c). Typhoon influences on atmospheric aerosol, caused by
269 varying factors such as wind speed and precipitation, have been studied in China (Yan et al.,
270 2016; Liu et al., 2018), Korea (Kim et al., 2007), Malaysia (Juneng et al., 2011), the South China
271 Sea (Reid et al., 2015, 2016b), and Taiwan (Fang et al., 2009; Chang et al., 2011; Lu et al.,
272 2017). The influences of typhoons on biomass burning emissions and transport in the MC have
273
274

275 also been examined (Reid et al., 2012; Wang et al., 2013). In this case, the influence of this storm
276 changed the prevailing wind direction approaching the northern Philippines, effectively pulling
277 an air mass from the west of the island, and along with it, emissions from continental East Asia
278 (Figure 2c). Furthermore, the air mass passed through regions of relatively little rainfall during
279 transport to the Philippines (Figure 2c), and accumulated rainfall at MO during this sample set
280 was very low (Table 1). One CALIPSO overpass around the ending time of set MO12 and one
281 during the nighttime after sampling ended (Figure 3) show that in the direction of transport (i.e.
282 north of the MO, from around 15-20° N), there is an aerosol layer extending up to around 2 km
283 during the day (northwest of MO) and 3 km at night (northeast of MO). The influence of
284 emissions from continental East Asia is also apparent in the NAAPS model (Figure 4c).
285 Observations at Dongsha Island, located to the north of the Philippines, have revealed influence
286 from Gobi Desert emissions (Wang et al., 2011) and anthropogenic sources (Atwood et al.,
287 2013). Farther south in the MC, aerosol measurements in Malaysia have also indicated influence
288 of aged, long-range transport from sites to the north in East Asia (Farren et al., 2019).

289

290 **3.1.4 MO14 (October 6 – 8, 2018): Mixed Influences**

291 The final MOUDI set (MO14) included in this study represents a transition in
292 meteorological regimes at the end of the SWM season and resulted in the highest overall water-
293 soluble mass concentration. This event had some of the lowest rainfall amounts in the region
294 surrounding Metro Manila (Figure 2d), with zero accumulated precipitation at MO during the
295 sampling period (Table 1). Furthermore, low cloud fraction was observed for regions to the
296 northwest and east of Metro Manila (Figure 1d). Back-trajectories from HYSPLIT show that the
297 air mass appeared to be influenced by a mix of continental sources in East Asia and local sources
298 (Figure 2d). Furthermore, two CALIPSO overpasses, one during the nighttime while sampling
299 was occurring and the other during the daytime after sampling ended, show a deep aerosol layer
300 north of MO, extending from the surface to around 2 km on October 6th and lower on October 8th
301 (Figure 3). From the NAAPS model, it appears that a mixture of MC smoke emissions and
302 continental East Asia emissions converge around the northern Philippines (Figure 4d).

303

304 **3.2. Ground-Based Aerosol Chemical Composition**

305 **3.2.1 Size-Resolved Aerosol Characteristics**

306 The water-soluble mass size distributions and the percent contribution of each MOUDI
307 stage to the water-soluble mass for the four sets of interest (MO7, MO12, MO14, and MO11)
308 and the average (\pm one standard deviation) of the remaining sets (MO1 – MO6, MO8 – MO10)
309 are shown in Figure 5. Most of the sets show a bimodal distribution with peaks in both the
310 submicrometer and supermicrometer range; one exception is the lowest aerosol event (MO11),
311 which shows a fairly broad size distribution. The highest aerosol event, MO14, shows a
312 significant peak in the submicrometer range, with a very large drop in mass concentration in the
313 supermicrometer range. This is in stark contrast to the lowest aerosol event (MO11), which
314 shows that the supermicrometer range contributes the greatest percent to the total water-soluble
315 mass. The second and third highest aerosol events, MO7 and MO12, also show significant
316 enhancements in the supermicrometer range as compared to the average of the other sets and
317 MO14.

318 Figure 6 describes the major species contributing to the water-soluble mass. MO14 had
319 one of the highest combined contributions of SO_4^{2-} and NH_4^+ (77.2% of water-soluble mass),
320 with only MO10 being slightly larger at 77.6%. These two species are typically associated with

321 the submicrometer range and anthropogenic origins due to their formation through secondary
322 processes such as gas-to-particle conversion of gaseous SO₂ and NH₃, respectively, and aqueous
323 processing to form SO₄²⁻ (Ervens, 2015). In contrast, MO11 had the lowest overall combined
324 percent contribution of these two species (41.4%) to the water-soluble aerosol mass. Of all 12
325 SWM MOUDI sets, MO11 had the highest percent contributions from Ca²⁺ (14.0%) and Cl⁻
326 (12.5%), as well as one of the highest contributions from Na⁺ (10.7%). Each of these species is
327 associated with primary emissions, including dust in the case of Ca²⁺ and sea salt for Na⁺ and Cl⁻,
328 resulting in larger particles (i.e. > 1 μm). The HYSPLIT back-trajectories for MO11 match well
329 with the MOUDI results, as the influence of marine aerosol (i.e. Na⁺, Cl⁻) and lack of
330 anthropogenic sources of SO₂ and NH₃ is apparent. Local sources of dust most likely contribute
331 the highest amount to the measured Ca²⁺, as the back-trajectories show few other crustal sources
332 farther upwind. Average size-resolved profiles for all of the species in these 12 sample sets can
333 be found in Cruz et al. (2019), with characteristic size distribution profiles agreeing with the
334 above assessments.

335

336 **3.2.2 Enhancements in Tracer Species**

337 In addition to insights from the major water-soluble chemical species found in aerosol,
338 tracer aerosol species can also be used to identify impacting emission sources (e.g. Fung and
339 Wong, 1995; Allen et al., 2001; Ma et al., 2019). For the aforementioned high aerosol events,
340 numerous tracer species are elevated in some, but not all, sample sets. This makes these species
341 prime candidates for linking influencing sources to the measured ambient aerosol. The authors
342 theorize that MO8, which was the 4th highest aerosol event (Table 1), also was impacted by
343 biomass burning due to the back-trajectory analysis (Figure S2), NAAPS model (Figure S4), and
344 increases in select species described subsequently. Therefore, MO8 was separated from the other
345 sample sets for the purposes of the following characterizations. Figure 7 shows the size-resolved
346 aerosol composition for select tracer species for the four highest aerosol events (MO7, MO8,
347 MO12, and MO14), the lowest aerosol event (MO11), and the average (± standard deviation) of
348 the remaining seven sample sets.

349 Potassium is frequently used as a biomass burning tracer (e.g. Andreae, 1983; Artaxo et
350 al., 1994; Echalar et al., 1995; Chow et al., 2004; Thepnuan et al., 2019). This species shows
351 highly elevated levels in the submicrometer range for MO7 and MO8 (i.e. the sets influenced by
352 biomass burning transport from the MC). Other elevated trace elements for these two profiles
353 include Rb, Cs, Se, and Ti (Figure 7). Previous studies in the western United States (Schlosser et
354 al., 2017; Ma et al., 2019) have also shown Rb enhancements in wildfire-influenced aerosol. Rb
355 has also been measured in flaming and smoldering biomass burning emissions (Yamasoe et al.,
356 2000). Enhancements in Rb and Cs in the fine fraction of aerosol influenced by wildfire
357 emissions have been observed in South Africa (Maenhaut et al., 1996), with similar results
358 shown in this study for aerosol in the submicrometer size range. Se is also enhanced for these
359 two sets in the submicrometer range, as it is often formed through gas-to-particle conversion
360 processes of inorganic Se compounds (Wen and Carignan, 2007). A wide variety of sources for
361 atmospheric Se exist (Mosher and Duce, 1987), including, but not limited to, coal combustion
362 (Thurston and Spengler, 1985; Fung and Wong, 1995; Song et al., 2001), marine emissions
363 (Arimoto et al., 1995), volcanos, and biomass burning (Mosher and Duce, 1987). In contrast to
364 the other enhanced species for MO7 and MO8, the mass concentration mode for Ti resides in
365 supermicrometer size range. Ti is typically associated with crustal material that can be suspended
366 through mechanisms such as vehicle usage (Sternbeck et al., 2002; Querol et al., 2008; Amato et

367 al., 2009) and lofting in wildfire plumes (Maudlin et al., 2015; Schlosser et al., 2017). While
368 long-range transport of biomass burning aerosol could lead to the enhancements measured for
369 these biomass burning tracer species, local emission sources, such as waste burning and wood
370 burning for cooking, may also play a role.

371 Two tracer species are included that showed enhancements for MO12, specifically Ba in
372 the supermicrometer range and V in the submicrometer range (Figure 7). One well-documented
373 source of aerosol Ba is non-exhaust vehicle emissions, including brakewear (Sternbeck et al.,
374 2002; Querol et al., 2008; Amato et al., 2009; Jeong et al., 2019). V also has well characterized
375 emission sources, most specifically fuel combustion (Fung and Wong, 1995; Artaxo et al., 1999;
376 Song et al., 2001; Lin et al., 2005; Kim and Hopke, 2008). In coastal environments, V is often
377 tied to shipping emissions (Agrawal et al., 2008; Pandolfi et al., 2011; Maudlin et al., 2015;
378 Mamoudou et al., 2018). As these sources are anthropogenic in origin, it is difficult to determine
379 the relative influences of long-range transport versus local emissions, especially with the
380 proximity of the sampling site to major roadways and shipping in Manila Bay. However, the
381 enhancement in V could result from the transport of the aerosol over major shipping lanes father
382 upwind.

383 Finally, Figure 7 shows three selected elements that appear enhanced in MO14, all of
384 which are typically tied to anthropogenic sources. Both Pb and Sn are found mainly in the
385 submicrometer range and have been linked by previous studies to vehicle emissions (Singh et al.,
386 2002; Amato et al., 2009), industrial emissions (Querol et al., 2008; Allen et al., 2001), and
387 waste burning (Kumar et al., 2015). Other sources of Pb could include E-waste recycling
388 (Fujimori et al., 2012) and biomass burning (Maenhaut et al., 1996). The size distribution of Mo
389 for MO14 shows a much broader distribution, with peaks in both the sub- and supermicrometer
390 ranges. Sources of Mo include vehicle emissions (Pakkanen et al., 2003; Amato et al., 2009),
391 combustion (Pakkanen et al., 2001, 2003), and industrial activity, including copper smelters
392 (Artaxo et al., 1999). As is the case with the enhanced species in MO12, the anthropogenic
393 nature of these species makes it difficult to determine the relative contribution of long-range
394 versus local emissions. However, as both MO12 and MO14 show enhancements in
395 anthropogenic-produced trace elements, the influence of long-range transport from industrial and
396 urban areas in continental East Asia is plausible.

397

398 **3.2.3 Variability of Water-Soluble Organic Species**

399 Figure 8 shows the sum of the total measured water-soluble organic species and the
400 relative contributions of oxalate, succinate, adipate, maleate, pyruvate, MSA, and phthalate to the
401 total measured water-soluble organics for MO7, MO8, MO11, MO12, MO14, and the average (\pm
402 one standard deviation) of the remaining sets. Malonate (C3) was not characterized due to its low
403 concentrations in the samples measured and the co-elution of C3 with carbonate in the IC
404 analysis. Glutarate (C5) was also excluded from the analysis due to very low concentrations. For
405 the examination of the organic species, MO8 was again separated from the other MOUDI sets
406 due to it having the second highest concentration of organic species ($0.66 \mu\text{g m}^{-3}$), and an organic
407 species contribution profile very similar to that of MO7. The remaining MOUDI sets included in
408 the average category (MO1 – MO6, MO9 – MO10) all have total organic species concentrations
409 that were less than the four highest aerosol sets (MO7, MO8, MO12, MO14) and greater than the
410 lowest aerosol set (MO11). The lowest aerosol event (MO11) has the lowest overall
411 concentration of organic aerosol ($0.09 \mu\text{g m}^{-3}$), while the 2nd highest aerosol event (MO7) has the
412 highest concentration of organic aerosol ($0.70 \mu\text{g m}^{-3}$).

413 Many studies worldwide have examined the relative contributions of organic species to
414 atmospheric aerosol, with oxalate typically having the highest contribution among dicarboxylic
415 acids (Kawamura and Kaplan, 1987; Kawamura and Ikushima, 1993; Kawamura and Sakaguchi,
416 1999; Sorooshian et al., 2007a; Hsieh et al., 2007, 2008; Aggarwal and Kawamura, 2008;
417 Deshmukh et al., 2012, 2018; Li et al., 2015; Hoque et al., 2017; Kunwar et al., 2019). Oxalate
418 was the dominant water-soluble organic species for all 12 MOUDI sets, with oxalate having the
419 highest contribution to the organic aerosol in MO12 (88.7% of total organic aerosol). Oxalate is
420 often considered a byproduct of photochemical aging of longer-chain dicarboxylic acids (e.g.
421 Kawamura and Ikushima, 1993; Kawamura and Sakaguchi, 1999), and therefore an increase in
422 oxalate is often considered a signature of aged aerosol in the absence of primary oxalate
423 emissions from sources such as biomass burning. Another major pathway of oxalate formation is
424 aqueous processing (Crahan et al., 2004; Ervens et al., 2004, 2018; Sorooshian et al., 2006,
425 2007b; Wonaschuetz et al., 2012), which is likely prevalent during the SWM when there is
426 frequent cloud cover. Previous studies have also demonstrated the ability for transport of and
427 photochemical aging of water-soluble organic acids over long distances in a marine environment
428 (e.g. Kawamura and Sakaguchi, 1999) and the importance of emissions from continental Asia in
429 the organic aerosol budget in the western north Pacific (Aggarwal and Kawamura, 2008; Hoque
430 et al., 2017). The back-trajectories of the air masses terminating at MO during MO12 and MO14
431 indicate origins of emissions from continental East Asia (Figure 2). It is plausible that the high
432 contribution of oxalate to the organic aerosol in MO12 and MO14 (which had the fourth highest
433 percent contribution of oxalate) is due to the degradation of both primarily-emitted and
434 secondarily-produced longer-chain dicarboxylic acids during the transport process through
435 mechanisms described above, such as photochemical degradation and aqueous processing, with
436 the former mechanism being plausible in the regions of low cloud cover to the north and
437 northwest of the Manila (Figure 1) and the latter mechanism potentially being of great
438 importance due to the typhoon influences during transport. While the aerosol measured in MO7
439 and MO8 also show long-range transport influences (Figure 2a and Figure S2), the overall signal
440 of organic aerosol is much stronger in these two sets, such that the absolute concentration of
441 oxalate (MO7: $0.47 \mu\text{g m}^{-3}$ and MO8: $0.42 \mu\text{g m}^{-3}$) is still greater than in MO12 ($0.19 \mu\text{g m}^{-3}$)
442 and MO14 ($0.37 \mu\text{g m}^{-3}$). However, biomass burning is a well-documented source of both
443 oxalate and longer-chain dicarboxylic acids (e.g. Falkovich et al., 2005; Nirmalkar et al., 2015;
444 Cheng et al., 2017; Deshmukh et al., 2018; Thepnuan et al., 2019).

445 Succinate has been linked to biomass burning emissions (Wang and Shooter, 2004;
446 Falkovich et al., 2005; Zhao et al., 2014; Balla et al., 2018), vehicular emissions (Kawamura and
447 Kaplan, 1987; Kawamura et al., 1996; Yao et al., 2004), and secondary production via
448 photochemical reactions of precursor organic compounds (Kawamura and Ikushima, 1993;
449 Kawamura et al., 1996; Kawamura and Sakaguchi, 1999). The two MO MOUDI sets thought to
450 have the most influence from biomass burning emissions (MO7 and MO8) had the highest
451 organic aerosol mass concentrations and the highest mass percent contributions of succinate to
452 the organic aerosol (MO7: 14.3% and MO8: 17.5%). In contrast, the next highest contribution of
453 succinate to the organic aerosol was 4.2% measured in MO5. These results agree with previous
454 studies in Northeast China that showed an increase in total organic aerosol mass concentration
455 and a strong increase (decrease) in the relative contribution of succinate (oxalate) during biomass
456 burning periods as opposed to non-biomass burning periods (Cao et al., 2017). Results from
457 California, USA also showed higher percent contributions of succinate to the water-soluble
458 organic aerosol during periods influenced by biomass burning (Maudlin et al., 2015).

459 MO11 had the second highest relative contribution of maleate (28.5% of water-soluble
460 organic aerosol) out of all 12 sample sets and had a much higher percent contribution as
461 compared to the four highest aerosol events (<2.5% for each of the following: MO7, MO8,
462 MO12, and MO14). Maleate is linked to the oxidation of aromatic hydrocarbons, usually from
463 anthropogenic sources such as vehicular emissions (Kawamura and Kaplan, 1987; Kunwar et al.,
464 2019). One explanation for this result could be the higher rainfall accumulation in and around the
465 study region during MO11 as compared to the three highest aerosol sets (Figure 2). Wet
466 scavenging could have removed aerosol from transported air masses during their journey towards
467 MO, thereby increasing the relative contribution of local sources to the measured aerosol in
468 MO11. Because of the reduced aging time associated with emissions from local sources, the
469 relative increase in the contribution of longer-chain dicarboxylic acids and the decrease in the
470 relative contribution of oxalate is plausible. Hsieh et al. (2008) showed in samples from Taiwan
471 that the relative contribution of oxalate to the organic acids was also higher during periods of
472 high aerosol loading as opposed to periods of moderate aerosol loading when the overall PM
473 concentration was lower. MO11, which showed air mass back-trajectories originating to the east
474 of the Philippines from the open Pacific (Figure 2b), had the lowest overall water-soluble PM
475 concentration, the lowest overall concentration of water-soluble organic acids, and the second
476 lowest percent contribution of oxalate to the organic acid mass (57.1%) of all the sets.

477 Phthalate is an aromatic dicarboxylic acid often linked to anthropogenic sources through
478 photochemical transformation of emissions from vehicles (Kawamura and Kaplan, 1987;
479 Kawamura and Ikushima, 1993) and waste burning (Kumar et al., 2015), although aqueous
480 processing has also been proposed as a formation mechanism (Kunwar et al., 2019).
481 Accordingly, phthalate has been shown to have seasonal and diurnal variations in concentration,
482 with enhanced production usually linked to times of stronger solar radiation (i.e. summertime
483 and daytime: Satsumabayashi et al., 1990; Ray and McDow, 2005; Ho et al., 2006; Kunwar et
484 al., 2019). However, increased emissions of precursor species during different times of the year
485 may affect these trends (Hyder et al., 2012). Sets MO7, MO8, MO11, and MO14 had the highest
486 contribution to the water-soluble organics from phthalate (range: 9.5 – 10.2%). In contrast, the
487 remaining sets had a much lower contribution (range: 1.7 – 4.9%). However, the absolute
488 concentration of phthalate was highest in sets MO7, MO8, and MO14 (range: 45.3 – 67.0 ng m⁻³),
489 and much lower for the remaining sets (range: 2.0 – 8.9 ng m⁻³). Increased phthalate
490 concentrations during biomass burning episodes have been previously measured in SE Asia (Cao
491 et al., 2017). Furthermore, cloud coverage was fairly low during MO14 as compared to the other
492 sets of interest (Figure 1), increasing the possibility of photochemical production of phthalate.
493 For the remaining sample sets, the range of phthalate concentrations is substantially lower and
494 fairly consistent, indicating that the measured phthalate in these samples most likely represents
495 the local background conditions.

496 While not a carboxylic acid, MSA is nonetheless an important organic aerosol species,
497 especially in marine environments. The assumed precursor of MSA in this study is from the
498 oxidation of marine-emitted dimethylsulfide (DMS). Interestingly, all sample sets showed
499 approximately the same mass percent contribution of MSA to the organic aerosol, ranging from a
500 minimum of 3.1% (MO6) to a maximum of 7.0% (MO5). However, the absolute concentration
501 of MSA was highest in the two sets with biomass burning influence (MO7: 23.3 ng m⁻³ and
502 MO8: 21.4 ng m⁻³), with concentrations 8.4 and 7.7 times higher, respectively, than the lowest
503 MSA concentration measured (MO11: 2.8 ng m⁻³). A previous study showed that MSA
504 concentrations in air masses with mixed influence from marine and biomass burning emissions

505 are higher than the concentrations measured from either source alone (Sorooshian et al., 2015).
506 The results from the present study (i.e. more MSA measured in sets with biomass burning
507 influence) in SE Asia again highlight the complexity of interactions between air masses with
508 different sources and the accompanying changes in aerosol physiochemical properties.
509

510 **4. Conclusions**

511 This study sought to characterize influences of local and long-range transported aerosol
512 to the Philippines during the Southwest Monsoon (SWM) season as well as the various synoptic
513 and local scale conditions that facilitate and suppress long-range transport of aerosol. As a highly
514 populated mega-city, Metro Manila is the source of a large amount of urban, anthropogenic
515 pollution. However, synoptic-scale weather, including the typical SWM flow and typhoons, can
516 impact the transport of aerosol to and from Metro Manila. While previous work in a rural area in
517 the northwest edge of the Philippines has identified seasonal aerosol transport patterns to the
518 Philippines using PM_{2.5} data (Bagtasa et al., 2018), the present study highlights case studies of in
519 situ size-resolved aerosol measurements from Metro Manila to examine the potential for aerosol
520 transport to impact this urban area as well.

521 For two of the sample sets with enhanced total water-soluble aerosol mass concentration,
522 biomass burning aerosol transport from the Maritime Continent (MC) towards the Philippines
523 was identified using air mass back-trajectories and the Navy Aerosol Analysis and Prediction
524 System (NAAPS) model. This transport followed a southwesterly flow pattern that is typical of
525 this time of year (Figure S2) and lends its name to the SWM season. Deep aerosol layers,
526 extending from the surface to 3 km, were identified by CALIOP to the southwest of the
527 Philippines. The influence on aerosol in Metro Manila was shown through enhancements in
528 biomass burning tracer species (e.g. K, Rb) and increased concentration of organic aerosol. The
529 challenges in satellite-based retrievals of biomass burning in the region (Reid et al., 2012, 2013)
530 and the underestimation of fire activity in the region by these satellite retrievals (Reid et al.,
531 2013) lead to unanswered questions about the amount and fate of biomass burning emissions in
532 the MC and SE Asia. The ability to measure biomass burning signatures in a highly polluted,
533 urban mega-city such as Metro Manila and the evidence of long-range transport gathered through
534 multiple methods and data sources (i.e. in situ measurements, models, and remote-sensing)
535 speaks to the strong signature of biomass burning emissions in the region and the long-range
536 transport pathways available for these emissions.

537 In contrast, transport of anthropogenic emissions from continental East Asia was
538 identified on two occasions with high water-soluble aerosol mass concentrations, with one
539 measured instance of long-range transport having been facilitated by the influence of a typhoon.
540 In these cases, it is difficult to separate urban emissions between local and distant sources.
541 However, the elevation of select tracer species (Ba, V, Pb, Mo, Sn) and the water-soluble organic
542 aerosol characteristics for these two cases (i.e. high relative contribution of oxalate to the organic
543 aerosol) indicated that long-range transported urban emissions could impact Metro Manila.

544 Finally, one low aerosol loading case was impacted by air masses travelling over the
545 open ocean to the east of the Philippines. This case showed an enhanced fraction of
546 supermicrometer aerosol and a very low concentration of water-soluble organic acids. Higher
547 rain accumulation during this sample set, as opposed to the sample sets with the highest water-
548 soluble aerosol concentrations, could have led to greater wet scavenging of aerosol. This case
549 also had the lowest overall mass concentration of water-soluble organic species, a low percent
550 contribution of oxalate to the water-soluble organics, and a high percent contribution of maleate.

551 This result points to the relative importance of locally-emitted species that have not yet
552 undergone photochemical and aqueous processing mechanisms that lead to the degradation of
553 longer-chain dicarboxylic acid species into oxalate.

554 These results have important implications for better understanding the aerosol budget in
555 and around the Philippines and SE Asia via the identification of various tracer species (e.g. K
556 and Rb for biomass burning) and the impacts of different long-range aerosol transport pathways.
557 In addition, the mixing of different air mass types, resulting in changes in aerosol characteristics
558 (e.g. enhanced oxalate in emissions from continental regions, enhanced MSA during periods of
559 biomass burning influence), is a subject that requires more attention on a global basis. While this
560 work has shown the influence of mixing biomass burning emissions and urban emissions, from
561 both local and more distant urban centers, additional analysis at the study site has demonstrated
562 the influences seen from the mixing of sea salt aerosol with other airmasses (AzadiAghdam et
563 al., 2019). As remote-sensing measurements in this region are notoriously difficult (e.g. Reid et
564 al., 2009, 2013), in situ and model results lend vital data to address the questions surrounding
565 characteristics of aerosol that are transported into and out of this highly-populated region.
566 Measurements from in situ airborne campaigns, such as CAMP²Ex, can further address the
567 changes in aerosol physicochemical characteristics that occur during long-range transport and
568 aging in the atmosphere in the region.

569
570 *Data availability:* Ground-based size-resolved aerosol data from the Manila Observatory can be
571 found at DOI:10.5067/Suborbital/CAMP2EX2018/DATA001

572
573 *Author Contribution:* MTC, MOC, JBS, RAB, ABM, CS, and AS designed the experiments and
574 all co-authors carried out some aspect of the data collection. MTC, RAB, CS, and AS conducted
575 data analysis and interpretation. RAB and AS prepared the manuscript with contributions from
576 all co-authors.

577
578 *Competing interests:* The authors declare that they have no conflict of interest.

579
580 *Acknowledgements:* This research was funded by NASA grant 80NSSC18K0148. R. A. Braun
581 acknowledges support from the ARCS Foundation. M. T. Cruz acknowledges support from the
582 Philippine Department of Science and Technology's ASTHRD Program. A. B. MacDonald
583 acknowledges support from the Mexican National Council for Science and Technology
584 (CONACYT). We acknowledge Agilent Technologies for their support and Shane Snyder's
585 laboratories for ICP-QQQ data.

586 587 **References**

588
589 Aggarwal, S. G., and Kawamura, K.: Molecular distributions and stable carbon isotopic
590 compositions of dicarboxylic acids and related compounds in aerosols from Sapporo, Japan:
591 Implications for photochemical aging during long-range atmospheric transport, *J. Geophys. Res.-*
592 *Atmos.*, 113, 10.1029/2007jd009365, 2008.

593
594 Agrawal, H., Malloy, Q. G. J., Welch, W. A., Wayne Miller, J., and Cocker, D. R.: In-use
595 gaseous and particulate matter emissions from a modern ocean going container vessel, *Atmos.*
596 *Environ.*, 42, 5504-5510, <https://doi.org/10.1016/j.atmosenv.2008.02.053>, 2008.

597
598 Akagi, S. K., Craven, J. S., Taylor, J. W., McMeeking, G. R., Yokelson, R. J., Burling, I. R.,
599 Urbanski, S. P., Wold, C. E., Seinfeld, J. H., Coe, H., Alvarado, M. J., and Weise, D. R.:
600 Evolution of trace gases and particles emitted by a chaparral fire in California, *Atmos. Chem.*
601 *Phys.*, 12, 1397-1421, 10.5194/acp-12-1397-2012, 2012.
602
603 Alas, H. D., Müller, T., Birmili, W., Kecorius, S., Cambaliza, M. O., Simpas, J. B. B., Cayetano,
604 M., Weinhold, K., Vallar, E., Galvez, M. C., and Wiedensohler, A.: Spatial Characterization of
605 Black Carbon Mass Concentration in the Atmosphere of a Southeast Asian Megacity: An Air
606 Quality Case Study for Metro Manila, Philippines, *Aerosol Air Qual. Res.*, 18, 2301-2317,
607 10.4209/aaqr.2017.08.0281, 2018.
608
609 Allen, A. G., Nemitz, E., Shi, J. P., Harrison, R. M., and Greenwood, J. C.: Size distributions of
610 trace metals in atmospheric aerosols in the United Kingdom, *Atmos. Environ.*, 35, 4581-4591,
611 [https://doi.org/10.1016/S1352-2310\(01\)00190-X](https://doi.org/10.1016/S1352-2310(01)00190-X), 2001.
612
613 Amato, F., Pandolfi, M., Viana, M., Querol, X., Alastuey, A., and Moreno, T.: Spatial and
614 chemical patterns of PM₁₀ in road dust deposited in urban environment, *Atmos. Environ.*, 43,
615 1650-1659, <https://doi.org/10.1016/j.atmosenv.2008.12.009>, 2009.
616
617 Andreae, M. O.: Soot Carbon and Excess Fine Potassium: Long-Range Transport of
618 Combustion-Derived Aerosols, *Science*, 220, 1148, 10.1126/science.220.4602.1148, 1983.
619
620 Arimoto, R., Duce, R. A., Ray, B. J., Ellis Jr, W. G., Cullen, J. D., and Merrill, J. T.: Trace
621 elements in the atmosphere over the North Atlantic, *J. Geophys. Res.-Atmos.*, 100, 1199-1213,
622 10.1029/94jd02618, 1995.
623
624 Artaxo, P., Gerab, F., Yamasoe, M. A., and Martins, J. V.: Fine mode aerosol composition at
625 three long-term atmospheric monitoring sites in the Amazon Basin, *J. Geophys. Res.-Atmos.*, 99,
626 22857-22868, 10.1029/94jd01023, 1994.
627
628 Artaxo, P., Oyola, P., and Martinez, R.: Aerosol composition and source apportionment in
629 Santiago de Chile, *Nucl. Instrum. Meth. B*, 150, 409-416, [https://doi.org/10.1016/S0168-](https://doi.org/10.1016/S0168-583X(98)01078-7)
630 [583X\(98\)01078-7](https://doi.org/10.1016/S0168-583X(98)01078-7), 1999.
631
632 Atwood, S. A., Reid, J. S., Kreidenweis, S. M., Cliff, S. S., Zhao, Y., Lin, N.-H., Tsay, S.-C.,
633 Chu, Y.-C., and Westphal, D. L.: Size resolved measurements of springtime aerosol particles
634 over the northern South China Sea, *Atmos. Environ.*, 78, 134-143,
635 <https://doi.org/10.1016/j.atmosenv.2012.11.024>, 2013.
636
637 Atwood, S. A., Reid, J. S., Kreidenweis, S. M., Blake, D. R., Jonsson, H. H., Lagrosas, N. D.,
638 Xian, P., Reid, E. A., Sessions, W. R., and Simpas, J. B.: Size-resolved aerosol and cloud
639 condensation nuclei (CCN) properties in the remote marine South China Sea – Part 1:
640 Observations and source classification, *Atmos. Chem. Phys.*, 17, 1105-1123, 10.5194/acp-17-
641 1105-2017, 2017.
642

643 AzadiAghdam, M., Braun, R. A., Edwards, E.-L., Bañaga, P. A., Cruz, M. T., Betito, G.,
644 Cambaliza, M. O., Dadashazar, H., Lorenzo, G. R., Ma, L., MacDonald, A. B., Nguyen, P.,
645 Simpas, J. B., Stahl, C., and Sorooshian, A.: On the nature of sea salt aerosol at a coastal
646 megacity: Insights from Manila, Philippines in Southeast Asia, *Atmos. Environ.*, 216, 116922,
647 <https://doi.org/10.1016/j.atmosenv.2019.116922>, 2019.

648 Bagtasa, G.: Effect of Synoptic Scale Weather Disturbance to Philippine Transboundary Oxone
649 Pollution using WRF-CHEM. *Int. J. Environ. Sci. Dev.*, 2, 402-405,
650 10.7763/IJESD.2011.V2.159, 2011.

651
652 Bagtasa, G., Cayetano, M. G., and Yuan, C. S.: Seasonal variation and chemical characterization
653 of PM_{2.5} in northwestern Philippines, *Atmos. Chem. Phys.*, 18, 4965-4980, 10.5194/acp-18-
654 4965-2018, 2018.

655
656 Balla, D., Voutsas, D., and Samara, C.: Study of polar organic compounds in airborne particulate
657 matter of a coastal urban city, *Environ. Sci. Pollut. R.*, 25, 12191-12205, 10.1007/s11356-017-
658 9993-2, 2018.

659
660 Bautista, A. T., Pabroa, P. C. B., Santos, F. L., Racho, J. M. D., and Quirit, L. L.: Carbonaceous
661 particulate matter characterization in an urban and a rural site in the Philippines, *Atmos. Pollut.*
662 *Res.*, 5, 245-252, <https://doi.org/10.5094/APR.2014.030>, 2014.

663
664 Bovallius, A., Bucht, B., Roffey, R., and Anäs, P.: Long-range air transmission of bacteria, *Appl.*
665 *Environ. Microb.*, 35, 1231, 1978.

666
667 Braun, R. A., Dadashazar, H., MacDonald, A. B., Aldhaif, A. M., Maudlin, L. C., Crosbie, E.,
668 Aghdam, M. A., Hossein Mardi, A., and Sorooshian, A.: Impact of Wildfire Emissions on
669 Chloride and Bromide Depletion in Marine Aerosol Particles, *Environ. Sci. Technol.*, 51, 9013-
670 9021, 10.1021/acs.est.7b02039, 2017.

671
672 Brito, J., Freney, E., Dominutti, P., Borbon, A., Haslett, S. L., Batenburg, A. M., Colomb, A.,
673 Dupuy, R., Denjean, C., Burnet, F., Bourriane, T., Deroubaix, A., Sellegri, K., Borrmann, S.,
674 Coe, H., Flamant, C., Knippertz, P., and Schwarzenboeck, A.: Assessing the role of
675 anthropogenic and biogenic sources on PM₁ over southern West Africa using aircraft
676 measurements, *Atmos. Chem. Phys.*, 18, 757-772, 10.5194/acp-18-757-2018, 2018.

677
678 Campbell, J. R., Reid, J. S., Westphal, D. L., Zhang, J., Tackett, J. L., Chew, B. N., Welton, E. J.,
679 Shimizu, A., Sugimoto, N., Aoki, K., and Winker, D. M.: Characterizing the vertical profile of
680 aerosol particle extinction and linear depolarization over Southeast Asia and the Maritime
681 Continent: The 2007–2009 view from CALIOP, *Atmos. Res.*, 122, 520-543,
682 <https://doi.org/10.1016/j.atmosres.2012.05.007>, 2013.

683
684 Cao, F., Zhang, S.-C., Kawamura, K., Liu, X., Yang, C., Xu, Z., Fan, M., Zhang, W., Bao, M.,
685 Chang, Y., Song, W., Liu, S., Lee, X., Li, J., Zhang, G., and Zhang, Y.-L.: Chemical
686 characteristics of dicarboxylic acids and related organic compounds in PM_{2.5} during biomass-

687 burning and non-biomass-burning seasons at a rural site of Northeast China, *Environ. Pollut.*,
688 231, 654-662, <https://doi.org/10.1016/j.envpol.2017.08.045>, 2017.
689

690 Cayan, E. O., Chen, T.-C., Argete, J. C., Yen, M.-C., and Nilo, P. D.: The Effect of Tropical
691 Cyclones on Southwest Monsoon Rainfall in the Philippines, *J. Meteorol. Soc. Jpn. Ser. II*, 89A,
692 123-139, 10.2151/jmsj.2011-A08, 2011.
693

694 Chang, L. T.-C., Tsai, J.-H., Lin, J.-M., Huang, Y.-S., and Chiang, H.-L.: Particulate matter and
695 gaseous pollutants during a tropical storm and air pollution episode in Southern Taiwan, *Atmos.*
696 *Res.*, 99, 67-79, <https://doi.org/10.1016/j.atmosres.2010.09.002>, 2011.
697

698 Cheng, C., Li, M., Chan, C. K., Tong, H., Chen, C., Chen, D., Wu, D., Li, L., Wu, C., Cheng, P.,
699 Gao, W., Huang, Z., Li, X., Zhang, Z., Fu, Z., Bi, Y., and Zhou, Z.: Mixing state of oxalic acid
700 containing particles in the rural area of Pearl River Delta, China: implications for the formation
701 mechanism of oxalic acid, *Atmos. Chem. Phys.*, 17, 9519-9533, 10.5194/acp-17-9519-2017,
702 2017.
703

704 Chow, J. C., Watson, J. G., Kuhns, H., Etyemezian, V., Lowenthal, D. H., Crow, D., Kohl, S. D.,
705 Engelbrecht, J. P., and Green, M. C.: Source profiles for industrial, mobile, and area sources in
706 the Big Bend Regional Aerosol Visibility and Observational study, *Chemosphere*, 54, 185-208,
707 <https://doi.org/10.1016/j.chemosphere.2003.07.004>, 2004.
708

709 Chuang, M.-T., Chang, S.-C., Lin, N.-H., Wang, J.-L., Sheu, G.-R., Chang, Y.-J., and Lee, C.-T.:
710 Aerosol chemical properties and related pollutants measured in Dongsha Island in the northern
711 South China Sea during 7-SEAS/Dongsha Experiment, *Atmos. Environ.*, 78, 82-92,
712 <https://doi.org/10.1016/j.atmosenv.2012.05.014>, 2013.
713

714 Crahan, K. K., Hegg, D., Covert, D. S., and Jonsson, H.: An exploration of aqueous oxalic acid
715 production in the coastal marine atmosphere, *Atmos. Environ.*, 38, 3757-3764,
716 <https://doi.org/10.1016/j.atmosenv.2004.04.009>, 2004.
717

718 Cruz, F. T., Narisma, G. T., Villafuerte, M. Q., Cheng Chua, K. U., and Olaguera, L. M.: A
719 climatological analysis of the southwest monsoon rainfall in the Philippines, *Atmos. Res.*, 122,
720 609-616, <https://doi.org/10.1016/j.atmosres.2012.06.010>, 2013.
721

722 Cruz, M. T., Bañaga, P. A., Betito, G., Braun, R. A., Stahl, C., Aghdam, M. A., Cambaliza, M.
723 O., Dadashazar, H., Hilario, M. R., Lorenzo, G. R., Ma, L., MacDonald, A. B., Pabroa, P. C.,
724 Yee, J. R., Simpas, J. B., and Sorooshian, A.: Size-resolved Composition and Morphology of
725 Particulate Matter During the Southwest Monsoon in Metro Manila, Philippines, *Atmos. Chem.*
726 *Phys.*, 19, 10675-10696, <https://doi.org/10.5194/acp-19-10675-2019>, 2019.
727

728 Dave, P., Bhushan, M., and Venkataraman, C.: Aerosols cause intraseasonal short-term
729 suppression of Indian monsoon rainfall, *Sci. Rep.-UK*, 7, 17347, 10.1038/s41598-017-17599-1,
730 2017.
731

732 Deshmukh, D. K., Deb, M. K., Hopke, P. K., and Tsai, Y. I.: Seasonal Characteristics of Water-
733 Soluble Dicarboxylates Associated with PM₁₀ in the Urban Atmosphere of Durg City, India,
734 *Aerosol Air Qual. Res.*, 12, 683-696, 10.4209/aaqr.2012.02.0040, 2012.
735
736 Deshmukh, D. K., Mozammel Haque, M., Kawamura, K., and Kim, Y.: Dicarboxylic acids,
737 oxocarboxylic acids and α -dicarbonyls in fine aerosols over central Alaska: Implications for
738 sources and atmospheric processes, *Atmos. Res.*, 202, 128-139,
739 <https://doi.org/10.1016/j.atmosres.2017.11.003>, 2018.
740
741 Duce, R. A., Liss, P. S., Merrill, J. T., Atlas, E. L., Buat-Menard, P., Hicks, B. B., Miller, J. M.,
742 Prospero, J. M., Arimoto, R., Church, T. M., Ellis, W., Galloway, J. N., Hansen, L., Jickells, T.
743 D., Knap, A. H., Reinhardt, K. H., Schneider, B., Soudine, A., Tokos, J. J., Tsunogai, S.,
744 Wollast, R., and Zhou, M.: The atmospheric input of trace species to the world ocean, *Global*
745 *Biogeochem. Cy.*, 5, 193-259, 10.1029/91gb01778, 1991.
746
747 Echalar, F., Gaudichet, A., Cachier, H., and Artaxo, P.: Aerosol emissions by tropical forest and
748 savanna biomass burning: Characteristic trace elements and fluxes, *Geophys. Res. Lett.*, 22,
749 3039-3042, 10.1029/95gl03170, 1995.
750
751 Ervens, B.: Modeling the Processing of Aerosol and Trace Gases in Clouds and Fogs, *Chem.*
752 *Rev.*, 115, 4157-4198, 10.1021/cr5005887, 2015.
753
754 Ervens, B., Feingold, G., Frost, G. J., and Kreidenweis, S. M.: A modeling study of aqueous
755 production of dicarboxylic acids: 1. Chemical pathways and speciated organic mass production,
756 *J. Geophys. Res.-Atmos.*, 109, 10.1029/2003jd004387, 2004.
757
758 Ervens, B., Sorooshian, A., Aldhaif, A. M., Shingler, T., Crosbie, E., Ziemba, L., Campuzano-
759 Jost, P., Jimenez, J. L., and Wisthaler, A.: Is there an aerosol signature of chemical cloud
760 processing?, *Atmos. Chem. Phys.*, 18, 16099-16119, 10.5194/acp-18-16099-2018, 2018.
761
762 Falkovich, A. H., Graber, E. R., Schkolnik, G., Rudich, Y., Maenhaut, W., and Artaxo, P.: Low
763 molecular weight organic acids in aerosol particles from Rondônia, Brazil, during the biomass-
764 burning, transition and wet periods, *Atmos. Chem. Phys.*, 5, 781-797, 10.5194/acp-5-781-2005,
765 2005.
766
767 Fang, G.-C., Lin, S.-J., Chang, S.-Y., and Chou, C.-C. K.: Effect of typhoon on atmospheric
768 particulates in autumn in central Taiwan, *Atmos. Environ.*, 43, 6039-6048,
769 <https://doi.org/10.1016/j.atmosenv.2009.08.033>, 2009.
770
771 Farren, N. J., Dunmore, R. E., Mead, M. I., Mohd Nadzir, M. S., Samah, A. A., Phang, S. M.,
772 Bandy, B. J., Sturges, W. T., and Hamilton, J. F.: Chemical characterisation of water-soluble
773 ions in atmospheric particulate matter on the east coast of Peninsular Malaysia, *Atmos. Chem.*
774 *Phys.*, 19, 1537-1553, 10.5194/acp-19-1537-2019, 2019.
775

776 Flannigan, M. D., Krawchuk, M. A., de Groot, W. J., Wotton, B. M., and Gowman, L. M.:
777 Implications of changing climate for global wildland fire, *Int. J. Wildland Fire*, 18, 483-507,
778 <https://doi.org/10.1071/WF08187>, 2009.
779

780 Flannigan, M., Cantin, A. S., de Groot, W. J., Wotton, M., Newbery, A., and Gowman, L. M.:
781 Global wildland fire season severity in the 21st century, *Forest Ecol. Manag.*, 294, 54-61,
782 <https://doi.org/10.1016/j.foreco.2012.10.022>, 2013.
783

784 Fujimori, T., Takigami, H., Agusa, T., Eguchi, A., Bekki, K., Yoshida, A., Terazono, A., and
785 Ballesteros, F. C.: Impact of metals in surface matrices from formal and informal electronic-
786 waste recycling around Metro Manila, the Philippines, and intra-Asian comparison, *J. Hazard.*
787 *Mater.*, 221-222, 139-146, <https://doi.org/10.1016/j.jhazmat.2012.04.019>, 2012.
788

789 Fung, Y. S., and Wong, L. W. Y.: Apportionment of air pollution sources by receptor models in
790 Hong Kong, *Atmos. Environ.*, 29, 2041-2048, [https://doi.org/10.1016/1352-2310\(94\)00239-H](https://doi.org/10.1016/1352-2310(94)00239-H),
791 1995.
792

793 Gadde, B., Bonnet, S., Menke, C., and Garivait, S.: Air pollutant emissions from rice straw open
794 field burning in India, Thailand and the Philippines, *Environ. Pollut.*, 157, 1554-1558,
795 <https://doi.org/10.1016/j.envpol.2009.01.004>, 2009.
796

797 Ge, C., Wang, J., Reid, J. S., Posselt, D. J., Xian, P., and Hyer, E.: Mesoscale modeling of smoke
798 transport from equatorial Southeast Asian Maritime Continent to the Philippines: First
799 comparison of ensemble analysis with in situ observations, *J. Geophys. Res.-Atmos.*, 122, 5380-
800 5398, doi:10.1002/2016JD026241, 2017.
801

802 Gelaro, R., McCarty, W., Suárez, M. J., Todling, R., Molod, A., Takacs, L., Randles, C. A.,
803 Darmenov, A., Bosilovich, M. G., Reichle, R., Wargan, K., Coy, L., Cullather, R., Draper, C.,
804 Akella, S., Buchard, V., Conaty, A., Silva, A. M. d., Gu, W., Kim, G.-K., Koster, R., Lucchesi,
805 R., Merkova, D., Nielsen, J. E., Partyka, G., Pawson, S., Putman, W., Rienecker, M., Schubert,
806 S. D., Sienkiewicz, M., and Zhao, B.: The Modern-Era Retrospective Analysis for Research and
807 Applications, Version 2 (MERRA-2), *J. Climate*, 30, 5419-5454, 10.1175/jcli-d-16-0758.1,
808 2017.
809

810 Global Modeling and Assimilation Office (GMAO): MERRA-2 inst3_3d_asm_Nv: 3d,3-
811 Hourly,Instantaneous,Model-Level,Assimilation,Assimilated Meteorological Fields V5.12.4,
812 Goddard Earth Sciences Data and Information Services Center (GES DISC),
813 10.5067/WWQSQ8IVFW8, 2015a.
814

815 Global Modeling and Assimilation Office (GMAO): MERRA-2 tavg1_2d_rad_Nx: 2d,1-
816 Hourly,Time-Averaged,Single-Level,Assimilation,Radiation Diagnostics V5.12.4, Goddard
817 Earth Sciences Data and Information Services Center (GES DISC), 10.5067/Q9QMY5PBNV1T,
818 2015b.
819

820 Goldstein, A. H., Koven, C. D., Heald, C. L., and Fung, I. Y.: Biogenic carbon and
821 anthropogenic pollutants combine to form a cooling haze over the southeastern United States, P.
822 Natl. Acad. Sci. USA, 106, 8835-8840, 10.1073/pnas.0904128106, 2009.
823
824 Graf, H. F., Yang, J., and Wagner, T. M.: Aerosol effects on clouds and precipitation during the
825 1997 smoke episode in Indonesia, *Atmos. Chem. Phys.*, 9, 743-756, 10.5194/acp-9-743-2009,
826 2009.
827
828 Ho, K. F., Lee, S. C., Cao, J. J., Kawamura, K., Watanabe, T., Cheng, Y., and Chow, J. C.:
829 Dicarboxylic acids, ketocarboxylic acids and dicarbonyls in the urban roadside area of Hong
830 Kong, *Atmos. Environ.*, 40, 3030-3040, <https://doi.org/10.1016/j.atmosenv.2005.11.069>, 2006.
831
832 Hogan, T. F., Liu, M., Ridout, J. A., Peng, M. S., Whitcomb, T. R., Ruston, B. C., Reynolds, C.
833 A., Eckermann, S. D., Moskaitis, J. R., Baker, N. L., McCormack, J. P., Viner, K. C., McLay, J.
834 G., Flatau, M. K., Xu, L., Chen, C., and Chang, S. W.: The Navy Global Environmental Model,
835 *Oceanography*, 27, 116-125, <https://doi.org/10.5670/oceanog.2014.73>, 2014.
836
837 Hong, Y., Hsu, K.-L., Sorooshian, S., and Gao, X.: Precipitation Estimation from Remotely
838 Sensed Imagery Using an Artificial Neural Network Cloud Classification System, *J. Appl.*
839 *Meteorol.*, 43, 1834-1853, 10.1175/jam2173.1, 2004.
840
841 Hoque, M. M. M., Kawamura, K., and Uematsu, M.: Spatio-temporal distributions of
842 dicarboxylic acids, ω -oxocarboxylic acids, pyruvic acid, α -dicarbonyls and fatty acids in the
843 marine aerosols from the North and South Pacific, *Atmos. Res.*, 185, 158-168,
844 <https://doi.org/10.1016/j.atmosres.2016.10.022>, 2017.
845
846 Hsieh, L.-Y., Kuo, S.-C., Chen, C.-L., and Tsai, Y. I.: Origin of low-molecular-weight
847 dicarboxylic acids and their concentration and size distribution variation in suburban aerosol,
848 *Atmos. Environ.*, 41, 6648-6661, <https://doi.org/10.1016/j.atmosenv.2007.04.014>, 2007.
849
850 Hsieh, L.-Y., Chen, C.-L., Wan, M.-W., Tsai, C.-H., and Tsai, Y. I.: Speciation and temporal
851 characterization of dicarboxylic acids in PM_{2.5} during a PM episode and a period of non-
852 episodic pollution, *Atmos. Environ.*, 42, 6836-6850,
853 <https://doi.org/10.1016/j.atmosenv.2008.05.021>, 2008.
854
855 Hyder, M., Genberg, J., Sandahl, M., Swietlicki, E., and Jönsson, J. Å.: Yearly trend of
856 dicarboxylic acids in organic aerosols from south of Sweden and source attribution, *Atmos.*
857 *Environ.*, 57, 197-204, <https://doi.org/10.1016/j.atmosenv.2012.04.027>, 2012.
858
859 Jeong, C.-H., Wang, J. M., Hilker, N., Deboisz, J., Sofowote, U., Su, Y., Noble, M., Healy, R. M.,
860 Munoz, T., Dabek-Zlotorzynska, E., Celo, V., White, L., Audette, C., Herod, D., and Evans, G.
861 J.: Temporal and spatial variability of traffic-related PM_{2.5} sources: Comparison of exhaust and
862 non-exhaust emissions, *Atmos. Environ.*, 198, 55-69,
863 <https://doi.org/10.1016/j.atmosenv.2018.10.038>, 2019.
864

865 Juneng, L., Latif, M. T., and Tangang, F.: Factors influencing the variations of PM10 aerosol
866 dust in Klang Valley, Malaysia during the summer, *Atmos. Environ.*, 45, 4370-4378,
867 <https://doi.org/10.1016/j.atmosenv.2011.05.045>, 2011.
868

869 Kawamura, K., and Ikushima, K.: Seasonal changes in the distribution of dicarboxylic acids in
870 the urban atmosphere, *Environ. Sci. Technol.*, 27, 2227-2235, 10.1021/es00047a033, 1993.
871

872 Kawamura, K., and Kaplan, I. R.: Motor exhaust emissions as a primary source for dicarboxylic
873 acids in Los Angeles ambient air, *Environ. Sci. Technol.*, 21, 105-110, 10.1021/es00155a014,
874 1987.
875

876 Kawamura, K., and Sakaguchi, F.: Molecular distributions of water soluble dicarboxylic acids in
877 marine aerosols over the Pacific Ocean including tropics, *J. Geophys. Res.-Atmos.*, 104, 3501-
878 3509, 10.1029/1998jd100041, 1999.
879

880 Kawamura, K., Kasukabe, H., and Barrie, L. A.: Source and reaction pathways of dicarboxylic
881 acids, ketoacids and dicarbonyls in arctic aerosols: One year of observations, *Atmos. Environ.*,
882 30, 1709-1722, [https://doi.org/10.1016/1352-2310\(95\)00395-9](https://doi.org/10.1016/1352-2310(95)00395-9), 1996.
883

884 Kecorius, S., Madueño, L., Vallar, E., Alas, H., Betito, G., Birmili, W., Cambaliza, M. O.,
885 Catipay, G., Gonzaga-Cayetano, M., Galvez, M. C., Lorenzo, G., Müller, T., Simpas, J. B.,
886 Tamayo, E. G., and Wiedensohler, A.: Aerosol particle mixing state, refractory particle number
887 size distributions and emission factors in a polluted urban environment: Case study of Metro
888 Manila, Philippines, *Atmos. Environ.*, 170, 169-183,
889 <https://doi.org/10.1016/j.atmosenv.2017.09.037>, 2017.
890

891 Kim, E., and Hopke, P. K.: Source characterization of ambient fine particles at multiple sites in
892 the Seattle area, *Atmos. Environ.*, 42, 6047-6056,
893 <https://doi.org/10.1016/j.atmosenv.2008.03.032>, 2008.
894

895 Kim, J. Y., Ghim, Y. S., Song, C. H., Yoon, S.-C., and Han, J. S.: Seasonal characteristics of air
896 masses arriving at Gosan, Korea, using fine particle measurements between November 2001 and
897 August 2003, *J. Geophys. Res.-Atmos.*, 112, 10.1029/2005jd006946, 2007.
898

899 Kim Oanh, N. T., Upadhyay, N., Zhuang, Y. H., Hao, Z. P., Murthy, D. V. S., Lestari, P.,
900 Villarin, J. T., Chengchua, K., Co, H. X., Dung, N. T., and Lindgren, E. S.: Particulate air
901 pollution in six Asian cities: Spatial and temporal distributions, and associated sources, *Atmos.*
902 *Environ.*, 40, 3367-3380, <https://doi.org/10.1016/j.atmosenv.2006.01.050>, 2006.
903

904 Kristiansen, N. I., Stohl, A., Olivie, D. J. L., Croft, B., Søvde, O. A., Klein, H., Christoudias, T.,
905 Kunkel, D., Leadbetter, S. J., Lee, Y. H., Zhang, K., Tsigaridis, K., Bergman, T., Evangelidou, N.,
906 Wang, H., Ma, P. L., Easter, R. C., Rasch, P. J., Liu, X., Pitari, G., Di Genova, G., Zhao, S. Y.,
907 Balkanski, Y., Bauer, S. E., Faluvegi, G. S., Kokkola, H., Martin, R. V., Pierce, J. R., Schulz, M.,
908 Shindell, D., Tost, H., and Zhang, H.: Evaluation of observed and modelled aerosol lifetimes
909 using radioactive tracers of opportunity and an ensemble of 19 global models, *Atmos. Chem.*
910 *Phys.*, 16, 3525-3561, 10.5194/acp-16-3525-2016, 2016.

911
912 Kumar, S., Aggarwal, S. G., Gupta, P. K., and Kawamura, K.: Investigation of the tracers for
913 plastic-enriched waste burning aerosols, *Atmos. Environ.*, 108, 49-58,
914 <https://doi.org/10.1016/j.atmosenv.2015.02.066>, 2015.
915
916 Kunwar, B., Kawamura, K., Fujiwara, S., Fu, P., Miyazaki, Y., and Pokhrel, A.: Dicarboxylic
917 acids, oxocarboxylic acids and α -dicarbonyls in atmospheric aerosols from Mt. Fuji, Japan:
918 Implication for primary emission versus secondary formation, *Atmos. Res.*, 221, 58-71,
919 <https://doi.org/10.1016/j.atmosres.2019.01.021>, 2019.
920
921 Latif, M. T., Othman, M., Idris, N., Juneng, L., Abdullah, A. M., Hamzah, W. P., Khan, M. F.,
922 Nik Sulaiman, N. M., Jewaratnam, J., Aghamohammadi, N., Sahani, M., Xiang, C. J., Ahamad,
923 F., Amil, N., Darus, M., Varkkey, H., Tangang, F., and Jaafar, A. B.: Impact of regional haze
924 towards air quality in Malaysia: A review, *Atmos. Environ.*, 177, 28-44,
925 <https://doi.org/10.1016/j.atmosenv.2018.01.002>, 2018.
926
927 Li, X.-d., Yang, Z., Fu, P., Yu, J., Lang, Y.-c., Liu, D., Ono, K., and Kawamura, K.: High
928 abundances of dicarboxylic acids, oxocarboxylic acids, and α -dicarbonyls in fine aerosols
929 (PM_{2.5}) in Chengdu, China during wintertime haze pollution, *Environ. Sci. Pollut. R.*, 22,
930 12902-12918, [10.1007/s11356-015-4548-x](https://doi.org/10.1007/s11356-015-4548-x), 2015.
931
932 Lin, C.-C., Chen, S.-J., Huang, K.-L., Hwang, W.-I., Chang-Chien, G.-P., and Lin, W.-Y.:
933 Characteristics of Metals in Nano/Ultrafine/Fine/Coarse Particles Collected Beside a Heavily
934 Trafficked Road, *Environ. Sci. Technol.*, 39, 8113-8122, [10.1021/es048182a](https://doi.org/10.1021/es048182a), 2005.
935
936 Lin, C. Y., Hsu, H. m., Lee, Y. H., Kuo, C. H., Sheng, Y. F., and Chu, D. A.: A new transport
937 mechanism of biomass burning from Indochina as identified by modeling studies, *Atmos. Chem.*
938 *Phys.*, 9, 7901-7911, [10.5194/acp-9-7901-2009](https://doi.org/10.5194/acp-9-7901-2009), 2009.
939
940 Lin, I. I., Chen, J.-P., Wong, G. T. F., Huang, C.-W., and Lien, C.-C.: Aerosol input to the South
941 China Sea: Results from the MODerate Resolution Imaging Spectro-radiometer, the Quick
942 Scatterometer, and the Measurements of Pollution in the Troposphere Sensor, *Deep-Sea Res. Pt.*
943 *II*, 54, 1589-1601, <https://doi.org/10.1016/j.dsr2.2007.05.013>, 2007.
944
945 Lindqvist, O., Johansson, K., Bringmark, L., Timm, B., Aastrup, M., Andersson, A., Hovsenius,
946 G., Håkanson, L., Iverfeldt, Å., and Meili, M.: Mercury in the Swedish environment — Recent
947 research on causes, consequences and corrective methods, *Water Air Soil Poll.*, 55, xi-261,
948 [10.1007/bf00542429](https://doi.org/10.1007/bf00542429), 1991.
949
950 Liu, W., Han, Y., Yin, Y., Duan, J., Gong, J., Liu, Z., and Xu, W.: An aerosol air pollution
951 episode affected by binary typhoons in east and central China, *Atmos. Pollut. Res.*, 9, 634-642,
952 <https://doi.org/10.1016/j.apr.2018.01.005>, 2018.
953
954 Liu, Y., Cai, W., Sun, C., Song, H., Cobb, K. M., Li, J., Leavitt, S. W., Wu, L., Cai, Q., Liu, R.,
955 Ng, B., Cherubini, P., Büentgen, U., Song, Y., Wang, G., Lei, Y., Yan, L., Li, Q., Ma, Y., Fang,
956 C., Sun, J., Li, X., Chen, D., and Linderholm, H. W.: Anthropogenic aerosols cause recent

957 pronounced weakening of Asian Summer Monsoon relative to last four centuries, *Geophys. Res.*
958 *Letts.*, 46, 10.1029/2019gl082497, 2019.

959

960 Lu, C.-C., Yuan, C.-S., and Li, T.-C.: How Aeolian Dust Deteriorate Ambient Particulate Air
961 Quality along an Expansive River Valley in Southern Taiwan? A Case Study of Typhoon
962 Doksuri, *Aerosol Air Qual. Res.*, 17, 2181-2196, 10.4209/aaqr.2017.08.0257, 2017.

963

964 Lynch, P., Reid, J. S., Westphal, D. L., Zhang, J., Hogan, T. F., Hyer, E. J., Curtis, C. A., Hegg,
965 D. A., Shi, Y., Campbell, J. R., Rubin, J. I., Sessions, W. R., Turk, F. J., and Walker, A. L.: An
966 11-year global gridded aerosol optical thickness reanalysis (v1.0) for atmospheric and climate
967 sciences, *Geosci. Model Dev.*, 9, 1489-1522, 10.5194/gmd-9-1489-2016, 2016.

968

969 Lyons, W. A., Dooley, J. C., and Whitby, K. T.: Satellite detection of long-range pollution
970 transport and sulfate aerosol hazes, *Atmos. Environ. (1967)*, 12, 621-631,
971 [https://doi.org/10.1016/0004-6981\(78\)90242-1](https://doi.org/10.1016/0004-6981(78)90242-1), 1978.

972

973 Ma, L., Dadashazar, H., Braun, R. A., MacDonald, A. B., Aghdam, M. A., Maudlin, L. C., and
974 Sorooshian, A.: Size-resolved Characteristics of Water-Soluble Particulate Elements in a Coastal
975 Area: Source Identification, Influence of Wildfires, and Diurnal Variability, *Atmos. Environ.*,
976 <https://doi.org/10.1016/j.atmosenv.2019.02.045>, 2019.

977

978 Maenhaut, W., Salma, I., Cafmeyer, J., Annegarn, H. J., and Andreae, M. O.: Regional
979 atmospheric aerosol composition and sources in the eastern Transvaal, South Africa, and impact
980 of biomass burning, *J. Geophys. Res.-Atmos.*, 101, 23631-23650, 10.1029/95jd02930, 1996.

981

982 Maki, T., Lee, K. C., Kawai, K., Onishi, K., Hong, C. S., Kurosaki, Y., Shinoda, M., Kai, K.,
983 Iwasaka, Y., Archer, S. D. J., Lacap-Bugler, D. C., Hasegawa, H., and Pointing, S. B.: Aeolian
984 dispersal of bacteria associated with desert dust and anthropogenic particles over continental and
985 oceanic surfaces, *J. Geophys. Res.-Atmos.*, 124, 10.1029/2018jd029597, 2019.

986

987 Mamoudou, I., Zhang, F., Chen, Q., Wang, P., and Chen, Y.: Characteristics of PM_{2.5} from ship
988 emissions and their impacts on the ambient air: A case study in Yangshan Harbor, Shanghai, *Sci.*
989 *Total Environ.*, 640-641, 207-216, <https://doi.org/10.1016/j.scitotenv.2018.05.261>, 2018.

990

991 Marple, V., Olson, B., Romay, F., Hudak, G., Geerts, S. M., and Lundgren, D.: Second
992 Generation Micro-Orifice Uniform Deposit Impactor, 120 MOUDI-II: Design, Evaluation, and
993 Application to Long-Term Ambient Sampling, *Aerosol Sci. Tech.*, 48, 427-433,
994 10.1080/02786826.2014.884274, 2014.

995

996 Maudlin, L. C., Wang, Z., Jonsson, H. H., and Sorooshian, A.: Impact of wildfires on size-
997 resolved aerosol composition at a coastal California site, *Atmos. Environ.*, 119, 59-68,
998 <https://doi.org/10.1016/j.atmosenv.2015.08.039>, 2015.

999

1000 Mosher, B. W., and Duce, R. A.: A global atmospheric selenium budget, *J. Geophys. Res.-*
1001 *Atmos.*, 92, 13289-13298, doi:10.1029/JD092iD11p13289, 1987.

1002

1003 Nguyen, P., Sellars, S., Thorstensen, A., Tao, Y., Ashouri, H., Braithwaite, D., Hsu, K., and
1004 Sorooshian, S.: Satellites Track Precipitation of Super Typhoon Haiyan, *Eos Trans. AGU*, 95,
1005 133-135, 10.1002/2014eo160002, 2014.

1006

1007 Nguyen, P., Shearer, E. J., Tran, H., Ombadi, M., Hayatbini, N., Palacios, T., Huynh, P.,
1008 Braithwaite, D., Updegraff, G., Hsu, K., Kuligowski, B., Logan, W. S., and Sorooshian, S.: The
1009 CHRS Data Portal, an easily accessible public repository for PERSIANN global satellite
1010 precipitation data, *Scientific Data*, 6, 180296, 10.1038/sdata.2018.296, 2019.

1011

1012 Nirmalkar, J., Deshmukh, D. K., Deb, M. K., Tsai, Y. I., and Sopajaree, K.: Mass loading and
1013 episodic variation of molecular markers in PM_{2.5} aerosols over a rural area in eastern central
1014 India, *Atmos. Environ.*, 117, 41-50, <https://doi.org/10.1016/j.atmosenv.2015.07.003>, 2015.

1015

1016 Nordø, J.: Long range transport of air pollutants in Europe and acid precipitation in Norway,
1017 *Water Air Soil Poll.*, 6, 199-217, 10.1007/bf00182865, 1976.

1018

1019 Pakkanen, T. A., Loukkola, K., Korhonen, C. H., Aurela, M., Mäkelä, T., Hillamo, R. E., Aarnio,
1020 P., Koskentalo, T., Kousa, A., and Maenhaut, W.: Sources and chemical composition of
1021 atmospheric fine and coarse particles in the Helsinki area, *Atmos. Environ.*, 35, 5381-5391,
1022 [https://doi.org/10.1016/S1352-2310\(01\)00307-7](https://doi.org/10.1016/S1352-2310(01)00307-7), 2001.

1023

1024 Pakkanen, T. A., Kerminen, V.-M., Loukkola, K., Hillamo, R. E., Aarnio, P., Koskentalo, T., and
1025 Maenhaut, W.: Size distributions of mass and chemical components in street-level and rooftop
1026 PM₁ particles in Helsinki, *Atmos. Environ.*, 37, 1673-1690, [https://doi.org/10.1016/S1352-2310\(03\)00011-6](https://doi.org/10.1016/S1352-2310(03)00011-6), 2003.

1027

1028

1029 Pandolfi, M., Gonzalez-Castanedo, Y., Alastuey, A., de la Rosa, J. D., Mantilla, E., de la Campa,
1030 A. S., Querol, X., Pey, J., Amato, F., and Moreno, T.: Source apportionment of PM₁₀ and PM_{2.5}
1031 at multiple sites in the strait of Gibraltar by PMF: impact of shipping emissions, *Environ. Sci.*
1032 *Pollut. R.*, 18, 260-269, 10.1007/s11356-010-0373-4, 2011.

1033

1034 Querol, X., Alastuey, A., Moreno, T., Viana, M. M., Castillo, S., Pey, J., Rodríguez, S.,
1035 Artiñano, B., Salvador, P., Sánchez, M., Garcia Dos Santos, S., Hecce Garraleta, M. D.,
1036 Fernandez-Patier, R., Moreno-Grau, S., Negral, L., Minguillón, M. C., Monfort, E., Sanz, M. J.,
1037 Palomo-Marín, R., Pinilla-Gil, E., Cuevas, E., de la Rosa, J., and Sánchez de la Campa, A.:
1038 Spatial and temporal variations in airborne particulate matter (PM₁₀ and PM_{2.5}) across Spain
1039 1999–2005, *Atmos. Environ.*, 42, 3964-3979, <https://doi.org/10.1016/j.atmosenv.2006.10.071>,
1040 2008.

1041

1042 Ray, J., and McDow, S. R.: Dicarboxylic acid concentration trends and sampling artifacts,
1043 *Atmos. Environ.*, 39, 7906-7919, <https://doi.org/10.1016/j.atmosenv.2005.09.024>, 2005.

1044

1045 Reid, J. S., Hyer, E. J., Prins, E. M., Westphal, D. L., Zhang, J., Wang, J., Christopher, S. A.,
1046 Curtis, C. A., Schmidt, C. C., Eleuterio, D. P., Richardson, K. A., and Hoffman, J. P.: Global
1047 Monitoring and Forecasting of Biomass-Burning Smoke: Description of and Lessons From the

1048 Fire Locating and Modeling of Burning Emissions (FLAMBE) Program, *IEEE J. Sel. Top.*
1049 *Appl.*, 2, 144-162, 10.1109/jstars.2009.2027443, 2009.
1050
1051 Reid, J. S., Xian, P., Hyer, E. J., Flatau, M. K., Ramirez, E. M., Turk, F. J., Sampson, C. R.,
1052 Zhang, C., Fukada, E. M., and Maloney, E. D.: Multi-scale meteorological conceptual analysis of
1053 observed active fire hotspot activity and smoke optical depth in the Maritime Continent, *Atmos.*
1054 *Chem. Phys.*, 12, 2117-2147, 10.5194/acp-12-2117-2012, 2012.
1055
1056 Reid, J. S., Hyer, E. J., Johnson, R. S., Holben, B. N., Yokelson, R. J., Zhang, J., Campbell, J. R.,
1057 Christopher, S. A., Di Girolamo, L., Giglio, L., Holz, R. E., Kearney, C., Miettinen, J., Reid, E.
1058 A., Turk, F. J., Wang, J., Xian, P., Zhao, G., Balasubramanian, R., Chew, B. N., Janjai, S.,
1059 Lagrosas, N., Lestari, P., Lin, N.-H., Mahmud, M., Nguyen, A. X., Norris, B., Oanh, N. T. K.,
1060 Oo, M., Salinas, S. V., Welton, E. J., and Liew, S. C.: Observing and understanding the
1061 Southeast Asian aerosol system by remote sensing: An initial review and analysis for the Seven
1062 Southeast Asian Studies (7SEAS) program, *Atmos. Res.*, 122, 403-468,
1063 <https://doi.org/10.1016/j.atmosres.2012.06.005>, 2013.
1064
1065 Reid, J. S., Lagrosas, N. D., Jonsson, H. H., Reid, E. A., Sessions, W. R., Simpas, J. B., Uy, S.
1066 N., Boyd, T. J., Atwood, S. A., Blake, D. R., Campbell, J. R., Cliff, S. S., Holben, B. N., Holz,
1067 R. E., Hyer, E. J., Lynch, P., Meinardi, S., Posselt, D. J., Richardson, K. A., Salinas, S. V.,
1068 Smirnov, A., Wang, Q., Yu, L., and Zhang, J.: Observations of the temporal variability in aerosol
1069 properties and their relationships to meteorology in the summer monsoonal South China Sea/East
1070 Sea: the scale-dependent role of monsoonal flows, the Madden–Julian Oscillation, tropical
1071 cyclones, squall lines and cold pools, *Atmos. Chem. Phys.*, 15, 1745-1768, 10.5194/acp-15-
1072 1745-2015, 2015.
1073
1074 Reid, J. S., Xian, P., Holben, B. N., Hyer, E. J., Reid, E. A., Salinas, S. V., Zhang, J., Campbell,
1075 J. R., Chew, B. N., Holz, R. E., Kuciauskas, A. P., Lagrosas, N., Posselt, D. J., Sampson, C. R.,
1076 Walker, A. L., Welton, E. J., and Zhang, C.: Aerosol meteorology of the Maritime Continent for
1077 the 2012 7SEAS southwest monsoon intensive study – Part 1: regional-scale phenomena, *Atmos.*
1078 *Chem. Phys.*, 16, 14041-14056, 10.5194/acp-16-14041-2016, 2016a.
1079
1080 Reid, J. S., Lagrosas, N. D., Jonsson, H. H., Reid, E. A., Atwood, S. A., Boyd, T. J., Ghate, V.
1081 P., Xian, P., Posselt, D. J., Simpas, J. B., Uy, S. N., Zaiger, K., Blake, D. R., Bucholtz, A.,
1082 Campbell, J. R., Chew, B. N., Cliff, S. S., Holben, B. N., Holz, R. E., Hyer, E. J., Kreidenweis,
1083 S. M., Kuciauskas, A. P., Lolli, S., Oo, M., Perry, K. D., Salinas, S. V., Sessions, W. R.,
1084 Smirnov, A., Walker, A. L., Wang, Q., Yu, L., Zhang, J., and Zhao, Y.: Aerosol meteorology of
1085 Maritime Continent for the 2012 7SEAS southwest monsoon intensive study – Part 2: Philippine
1086 receptor observations of fine-scale aerosol behavior, *Atmos. Chem. Phys.*, 16, 14057-14078,
1087 10.5194/acp-16-14057-2016, 2016b.
1088
1089 Ross, A. D., Holz, R. E., Quinn, G., Reid, J. S., Xian, P., Turk, F. J., and Posselt, D. J.: Exploring
1090 the first aerosol indirect effect over Southeast Asia using a 10-year collocated MODIS, CALIOP,
1091 and model dataset, *Atmos. Chem. Phys.*, 18, 12747-12764, 10.5194/acp-18-12747-2018, 2018.
1092

1093 Satsumabayashi, H., Kurita, H., Yokouchi, Y., and Ueda, H.: Photochemical formation of
1094 particulate dicarboxylic acids under long-range transport in central Japan, *Atmos. Environ. Part*
1095 *A. General Topics*, 24, 1443-1450, [https://doi.org/10.1016/0960-1686\(90\)90053-P](https://doi.org/10.1016/0960-1686(90)90053-P), 1990.
1096

1097 Schlosser, J. S., Braun, R. A., Bradley, T., Dadashazar, H., MacDonald, A. B., Aldhaif, A. A.,
1098 Aghdam, M. A., Mardi, A. H., Xian, P., and Sorooshian, A.: Analysis of aerosol composition
1099 data for western United States wildfires between 2005 and 2015: Dust emissions, chloride
1100 depletion, and most enhanced aerosol constituents, *J. Geophys. Res.-Atmos.*, 122, 8951-8966,
1101 10.1002/2017jd026547, 2017.
1102

1103 Simpas, J., Lorenzo, G., and Cruz, M. T.: Monitoring Particulate Matter Levels and Composition
1104 for Source Apportionment Study in Metro Manila, Philippines, in: *Improving Air Quality in*
1105 *Asian Developing Countries: Compilation of Research Findings*, edited by: Kim Oanh, N. T.,
1106 NARENCA, Vietnam Publishing House of Natural Resources, Environment and Cartography,
1107 Vietnam, 239-261, 2014.
1108

1109 Singh, M., Jaques, P. A., and Sioutas, C.: Size distribution and diurnal characteristics of particle-
1110 bound metals in source and receptor sites of the Los Angeles Basin, *Atmos. Environ.*, 36, 1675-
1111 1689, [https://doi.org/10.1016/S1352-2310\(02\)00166-8](https://doi.org/10.1016/S1352-2310(02)00166-8), 2002.
1112

1113 Song, J., Zhao, Y., Zhang, Y., Fu, P., Zheng, L., Yuan, Q., Wang, S., Huang, X., Xu, W., Cao,
1114 Z., Gromov, S., and Lai, S.: Influence of biomass burning on atmospheric aerosols over the
1115 western South China Sea: Insights from ions, carbonaceous fractions and stable carbon isotope
1116 ratios, *Environ. Pollut.*, 242, 1800-1809, <https://doi.org/10.1016/j.envpol.2018.07.088>, 2018.
1117

1118 Song, X.-H., Polissar, A. V., and Hopke, P. K.: Sources of fine particle composition in the
1119 northeastern US, *Atmos. Environ.*, 35, 5277-5286, [https://doi.org/10.1016/S1352-](https://doi.org/10.1016/S1352-2310(01)00338-7)
1120 [2310\(01\)00338-7](https://doi.org/10.1016/S1352-2310(01)00338-7), 2001.
1121

1122 Sorooshian, A., Varutbangkul, V., Brechtel, F. J., Ervens, B., Feingold, G., Bahreini, R.,
1123 Murphy, S. M., Holloway, J. S., Atlas, E. L., Buzorius, G., Jonsson, H., Flagan, R. C., and
1124 Seinfeld, J. H.: Oxalic acid in clear and cloudy atmospheres: Analysis of data from International
1125 Consortium for Atmospheric Research on Transport and Transformation 2004, *J. Geophys. Res.-*
1126 *Atmos.*, 111, 10.1029/2005jd006880, 2006.
1127

1128 Sorooshian, A., Ng, N. L., Chan, A. W. H., Feingold, G., Flagan, R. C., and Seinfeld, J. H.:
1129 Particulate organic acids and overall water-soluble aerosol composition measurements from the
1130 2006 Gulf of Mexico Atmospheric Composition and Climate Study (GoMACCS), *J. Geophys.*
1131 *Res.-Atmos.*, 112, 10.1029/2007jd008537, 2007a.
1132

1133 Sorooshian, A., Lu, M.-L., Brechtel, F. J., Jonsson, H., Feingold, G., Flagan, R. C., and Seinfeld,
1134 J. H.: On the Source of Organic Acid Aerosol Layers above Clouds, *Environ. Sci. Technol.*, 41,
1135 4647-4654, 10.1021/es0630442, 2007b.
1136

1137 Sorooshian, A., Crosbie, E., Maudlin, L. C., Youn, J.-S., Wang, Z., Shingler, T., Ortega, A. M.,
1138 Hersey, S., and Woods, R. K.: Surface and airborne measurements of organosulfur and

1139 methanesulfonate over the western United States and coastal areas, *J. Geophys. Res.-Atmos.*,
1140 120, 8535-8548, 10.1002/2015jd023822, 2015.
1141
1142 Stein, A. F., Draxler, R. R., Rolph, G. D., Stunder, B. J. B., Cohen, M. D., and Ngan, F.:
1143 NOAA's HYSPLIT Atmospheric Transport and Dispersion Modeling System, *B. Am. Meteorol.*
1144 *Soc.*, 96, 2059-2077, 10.1175/bams-d-14-00110.1, 2015.
1145
1146 Sternbeck, J., Sjödin, Å., and Andréasson, K.: Metal emissions from road traffic and the
1147 influence of resuspension—results from two tunnel studies, *Atmos. Environ.*, 36, 4735-4744,
1148 [https://doi.org/10.1016/S1352-2310\(02\)00561-7](https://doi.org/10.1016/S1352-2310(02)00561-7), 2002.
1149
1150 Thepnuan, D., Chantara, S., Lee, C.-T., Lin, N.-H., and Tsai, Y. I.: Molecular markers for
1151 biomass burning associated with the characterization of PM_{2.5} and component sources during
1152 dry season haze episodes in Upper South East Asia, *Sci. Total Environ.*, 658, 708-722,
1153 <https://doi.org/10.1016/j.scitotenv.2018.12.201>, 2019.
1154
1155 Thurston, G. D., and Spengler, J. D.: A quantitative assessment of source contributions to
1156 inhalable particulate matter pollution in metropolitan Boston, *Atmos. Environ.*, 19, 9-25,
1157 [https://doi.org/10.1016/0004-6981\(85\)90132-5](https://doi.org/10.1016/0004-6981(85)90132-5), 1985.
1158
1159 Vaughan, M. A., Young, S. A., Winker, D. M., Powell, K. A., Omar, A. H., Liu, Z., Hu, Y., and
1160 Hostetler, C. A.: Fully automated analysis of space-based lidar data: an overview of the
1161 CALIPSO retrieval algorithms and data products, *Proc. SPIE*, 5575,
1162 <https://doi.org/10.1117/12.572024>, 2004.
1163
1164 Wang, H., and Shooter, D.: Low molecular weight dicarboxylic acids in PM₁₀ in a city with
1165 intensive solid fuel burning, *Chemosphere*, 56, 725-733,
1166 <https://doi.org/10.1016/j.chemosphere.2004.04.030>, 2004.
1167
1168 Wang, J., Ge, C., Yang, Z., Hyer, E. J., Reid, J. S., Chew, B.-N., Mahmud, M., Zhang, Y., and
1169 Zhang, M.: Mesoscale modeling of smoke transport over the Southeast Asian Maritime
1170 Continent: Interplay of sea breeze, trade wind, typhoon, and topography, *Atmos. Res.*, 122, 486-
1171 503, <https://doi.org/10.1016/j.atmosres.2012.05.009>, 2013.
1172
1173 Wang, S.-H., Tsay, S.-C., Lin, N.-H., Hsu, N. C., Bell, S. W., Li, C., Ji, Q., Jeong, M.-J.,
1174 Hansell, R. A., Welton, E. J., Holben, B. N., Sheu, G.-R., Chu, Y.-C., Chang, S.-C., Liu, J.-J.,
1175 and Chiang, W.-L.: First detailed observations of long-range transported dust over the northern
1176 South China Sea, *Atmos. Environ.*, 45, 4804-4808,
1177 <https://doi.org/10.1016/j.atmosenv.2011.04.077>, 2011.
1178
1179 Weber, R. J., Sullivan, A. P., Peltier, R. E., Russell, A., Yan, B., Zheng, M., de Gouw, J.,
1180 Warneke, C., Brock, C., Holloway, J. S., Atlas, E. L., and Edgerton, E.: A study of secondary
1181 organic aerosol formation in the anthropogenic-influenced southeastern United States, *J.*
1182 *Geophys. Res.-Atmos.*, 112, 10.1029/2007jd008408, 2007.
1183

1184 Wen, H., and Carignan, J.: Reviews on atmospheric selenium: Emissions, speciation and fate,
1185 Atmos. Environ., 41, 7151-7165, <https://doi.org/10.1016/j.atmosenv.2007.07.035>, 2007.
1186

1187 Winker, D. M., Vaughan, M. A., Omar, A., Hu, Y., Powell, K. A., Liu, Z., Hunt, W. H., and
1188 Young, S. A.: Overview of the CALIPSO Mission and CALIOP Data Processing Algorithms, J.
1189 Atmos. Ocean. Tech., 26, 2310-2323, [10.1175/2009jtech1281.1](https://doi.org/10.1175/2009jtech1281.1), 2009.
1190

1191 Wonaschuetz, A., Sorooshian, A., Ervens, B., Chuang, P. Y., Feingold, G., Murphy, S. M., de
1192 Gouw, J., Warneke, C., and Jonsson, H. H.: Aerosol and gas re-distribution by shallow cumulus
1193 clouds: An investigation using airborne measurements, J. Geophys. Res.-Atmos., 117,
1194 [10.1029/2012jd018089](https://doi.org/10.1029/2012jd018089), 2012.
1195

1196 Xian, P., Reid, J. S., Atwood, S. A., Johnson, R. S., Hyer, E. J., Westphal, D. L., and Sessions,
1197 W.: Smoke aerosol transport patterns over the Maritime Continent, Atmos. Res., 122, 469-485,
1198 <https://doi.org/10.1016/j.atmosres.2012.05.006>, 2013.
1199

1200 Xu, J., Zhang, J., Liu, J., Yi, K., Xiang, S., Hu, X., Wang, Y., Tao, S., and Ban-Weiss, G.:
1201 Influence of cloud microphysical processes on black carbon wet removal, global distributions,
1202 and radiative forcing, Atmos. Chem. Phys., 19, 1587-1603, [10.5194/acp-19-1587-2019](https://doi.org/10.5194/acp-19-1587-2019), 2019.
1203

1204 Yamasoe, M. A., Artaxo, P., Miguel, A. H., and Allen, A. G.: Chemical composition of aerosol
1205 particles from direct emissions of vegetation fires in the Amazon Basin: water-soluble species
1206 and trace elements, Atmos. Environ., 34, 1641-1653, [https://doi.org/10.1016/S1352-](https://doi.org/10.1016/S1352-2310(99)00329-5)
1207 [2310\(99\)00329-5](https://doi.org/10.1016/S1352-2310(99)00329-5), 2000.
1208

1209 Yan, J., Chen, L., Lin, Q., Zhao, S., and Zhang, M.: Effect of typhoon on atmospheric aerosol
1210 particle pollutants accumulation over Xiamen, China, Chemosphere, 159, 244-255,
1211 <https://doi.org/10.1016/j.chemosphere.2016.06.006>, 2016.
1212

1213 Yao, X., Fang, M., Chan, C. K., Ho, K. F., and Lee, S. C.: Characterization of dicarboxylic acids
1214 in PM_{2.5} in Hong Kong, Atmos. Environ., 38, 963-970,
1215 <https://doi.org/10.1016/j.atmosenv.2003.10.048>, 2004.
1216

1217 Yokelson, R. J., Crouse, J. D., DeCarlo, P. F., Karl, T., Urbanski, S., Atlas, E., Campos, T.,
1218 Shinozuka, Y., Kapustin, V., Clarke, A. D., Weinheimer, A., Knapp, D. J., Montzka, D. D.,
1219 Holloway, J., Weibring, P., Flocke, F., Zheng, W., Toohey, D., Wennberg, P. O., Wiedinmyer,
1220 C., Mauldin, L., Fried, A., Richter, D., Walega, J., Jimenez, J. L., Adachi, K., Buseck, P. R.,
1221 Hall, S. R., and Shetter, R.: Emissions from biomass burning in the Yucatan, Atmos. Chem.
1222 Phys., 9, 5785-5812, [10.5194/acp-9-5785-2009](https://doi.org/10.5194/acp-9-5785-2009), 2009.
1223

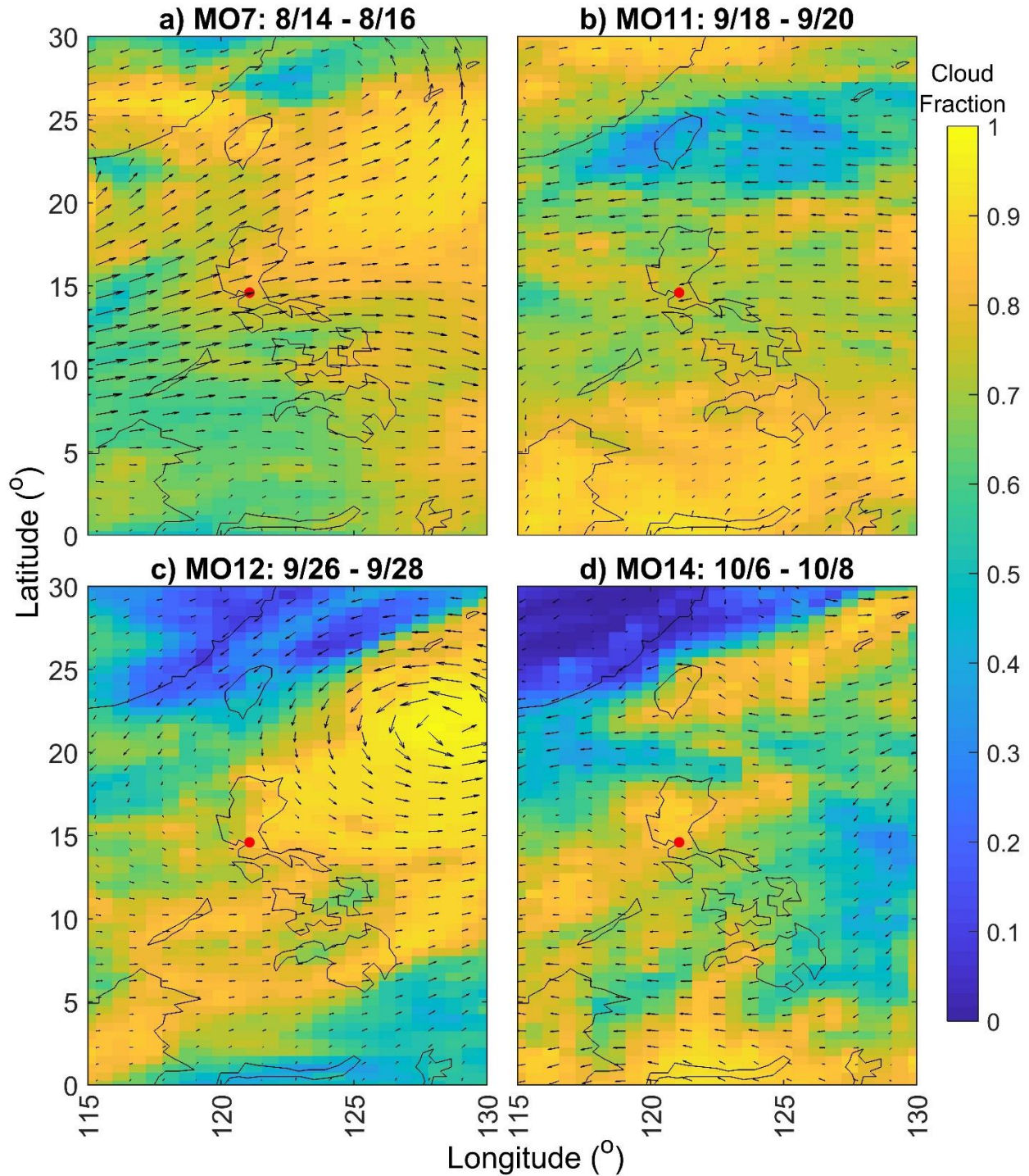
1224 Zhang, Y.-N., Zhang, Z.-S., Chan, C.-Y., Engling, G., Sang, X.-F., Shi, S., and Wang, X.-M.:
1225 Levoglucosan and carbonaceous species in the background aerosol of coastal southeast China:
1226 case study on transport of biomass burning smoke from the Philippines, Environ. Sci. Pollut. R.,
1227 19, 244-255, [10.1007/s11356-011-0548-7](https://doi.org/10.1007/s11356-011-0548-7), 2012.
1228

1229 Zhao, X., Wang, X., Ding, X., He, Q., Zhang, Z., Liu, T., Fu, X., Gao, B., Wang, Y., Zhang, Y.,
1230 Deng, X., and Wu, D.: Compositions and sources of organic acids in fine particles (PM_{2.5}) over
1231 the Pearl River Delta region, south China, *J. Environ. Sci.*, 26, 110-121,
1232 [https://doi.org/10.1016/S1001-0742\(13\)60386-1](https://doi.org/10.1016/S1001-0742(13)60386-1), 2014.

1233
1234
1235
1236

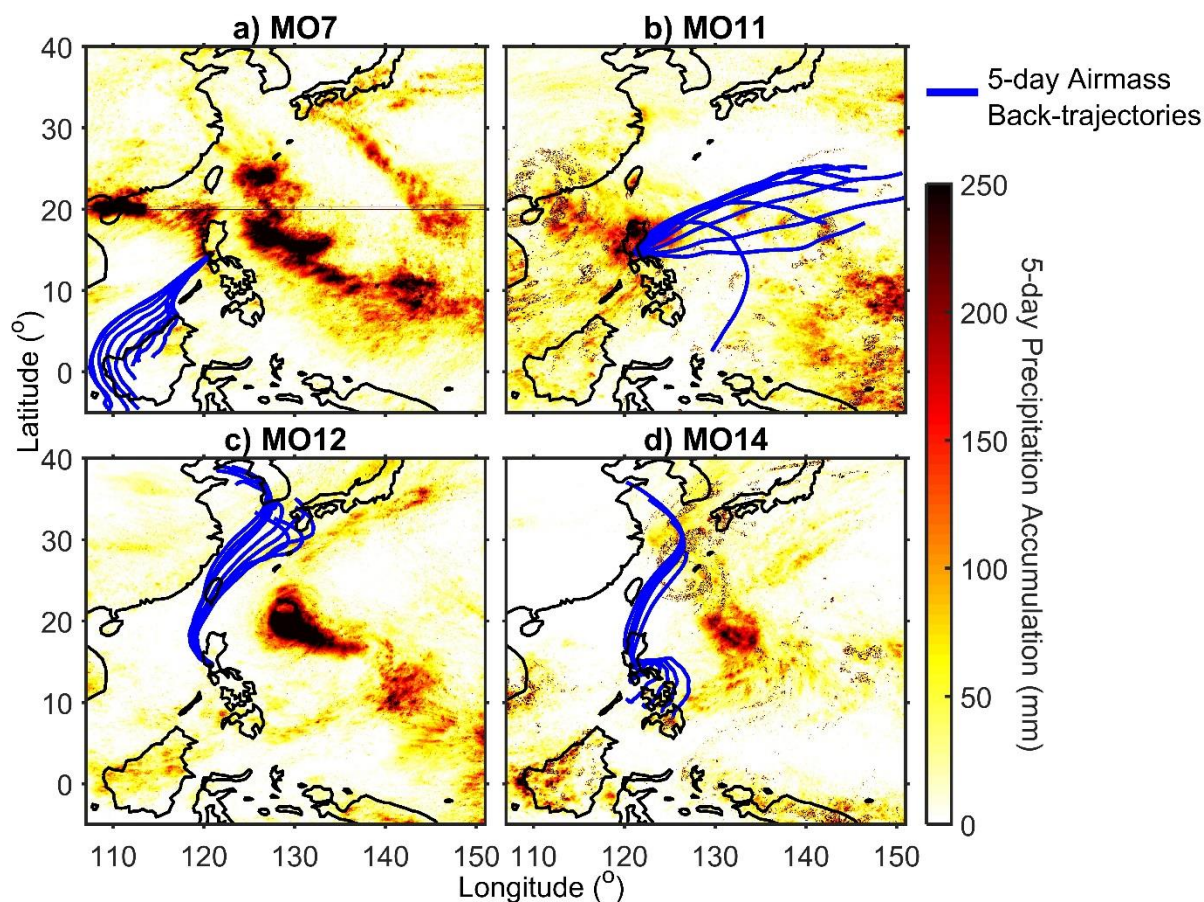
Table 1. Description of the MOUDI sample sets from this study. Accumulated precipitation during the sample sets was found using PERSIANN-CCS for the area bounded by: 121.0199 - 121.0968° E and 14.6067 - 14.6946° N.

Set Name	Start Date/ Local Time	End Date/ Local Time	Total Water-Soluble Species ($\mu\text{g m}^{-3}$)	% of water- soluble mass < 1 μm	Precipitation (mm)
MO1	7/19/18 12:40 PM	7/20/18 12:43 PM	4.61	67.3%	27
MO2	7/23/18 11:29 AM	7/25/18 5:10 PM	6.52	62.1%	14
MO4	7/25/18 7:16 PM	7/30/18 6:12 PM	5.17	66.4%	35
MO5	7/30/18 7:17 PM	8/1/18 1:19 PM	9.17	64.8%	11
MO6	8/6/18 2:33 PM	8/8/18 2:38 PM	5.11	55.8%	50
MO7	8/14/18 1:59 PM	8/16/18 2:04 PM	13.70	60.3%	3
MO8	8/22/18 1:46 PM	8/24/18 1:53 PM	12.73	71.6%	10
MO9	9/1/18 5:00 AM	9/3/18 5:05 AM	6.23	76.7%	64
MO10	9/10/18 2:42 PM	9/12/18 3:02 PM	6.36	79.5%	20
MO11	9/18/18 2:12 PM	9/20/18 2:24 PM	2.70	47.3%	26
MO12	9/26/18 1:53 PM	9/28/18 1:53 PM	13.49	59.9%	1
MO14	10/6/18 5:00 AM	10/8/18 5:05 AM	16.55	78.4%	0

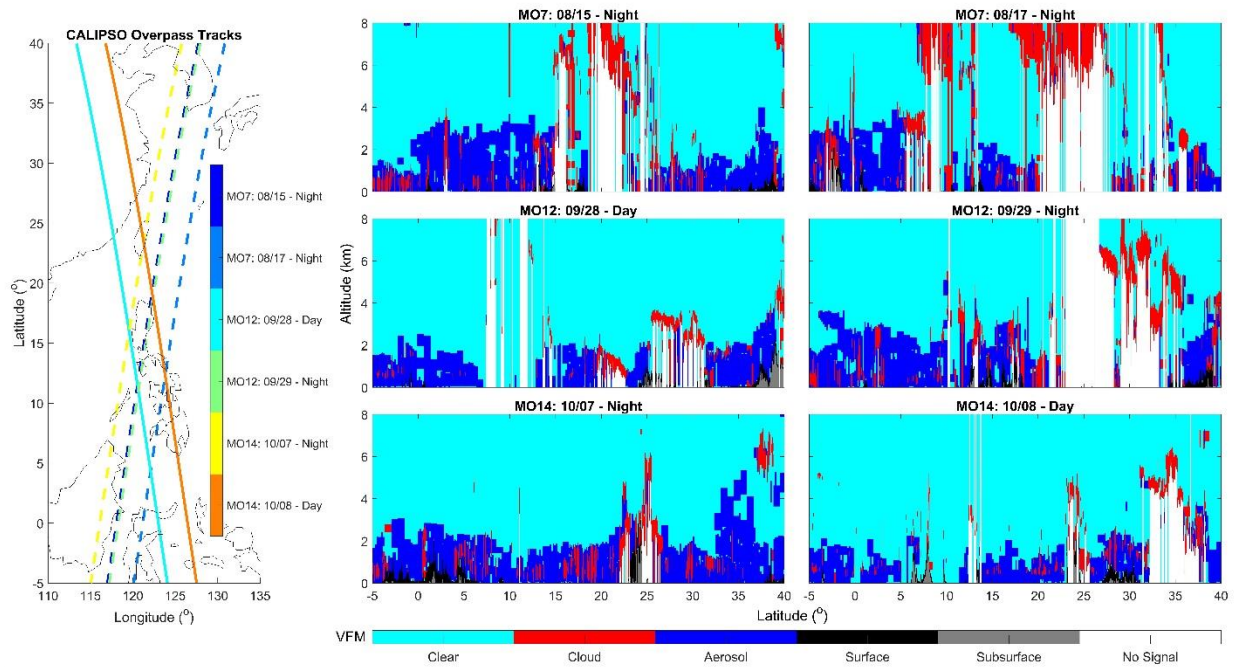


1237
 1238
 1239
 1240
 1241
 1242

Figure 1. MERRA-2 data for 850 hPa wind vectors and total cloud fraction averaged over the sample set duration for a) MO7 (8/14 – 8/16), b) MO11 (9/18 – 9/20), c) MO12 (9/26 – 9/28), and d) MO14 (10/6 – 10/8). The location of the Manila Observatory is indicated by the red circle. (Note that 850 hPa wind vectors are also averaged to increase grid spacing and improve figure readability.)

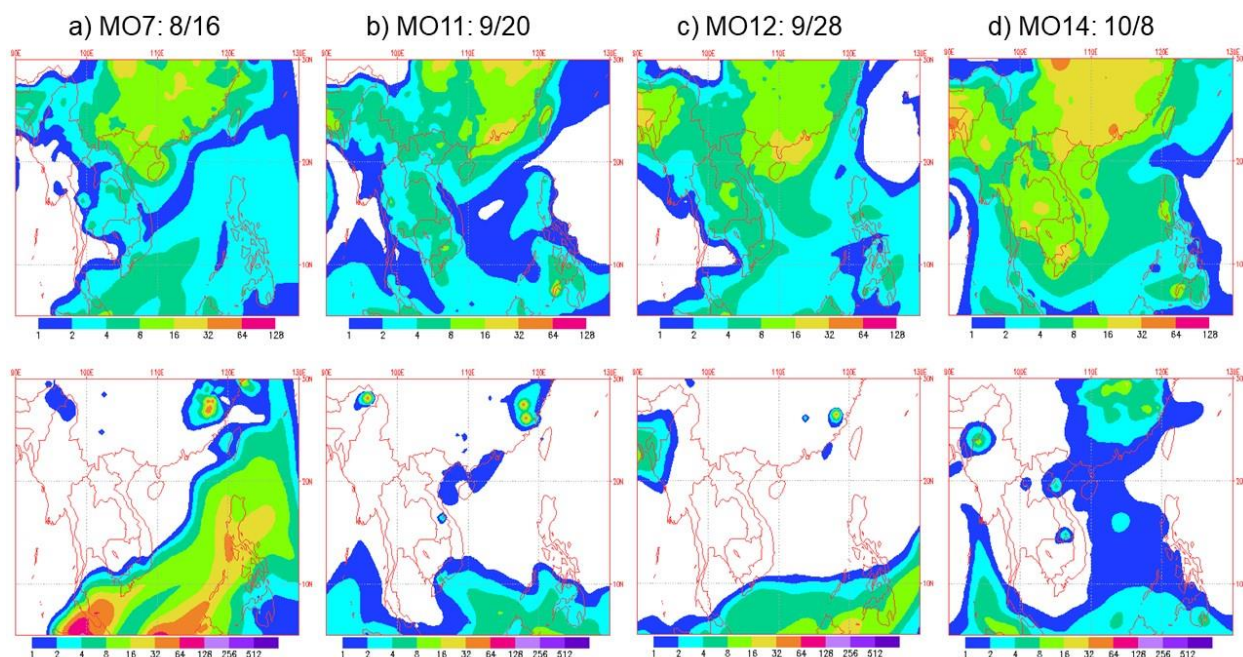


1243
 1244 **Figure 2.** Rainfall accumulation, extending from 5 days before the midpoint of each sample set
 1245 until the midpoint of each sample set, from PERSIAN-CCS for a) MO7, b) MO11, c) MO12, and
 1246 d) MO14. In blue are the 5-day air mass back-trajectories terminating at the MOUDI inlet at MO
 1247 (~85 m above sea level) every 6 h during each of the sample study periods. Note that the
 1248 maximum precipitation accumulation in the region shown during the study periods was 955 mm;
 1249 however, for figure readability, the scale was reduced to 0-250 mm.

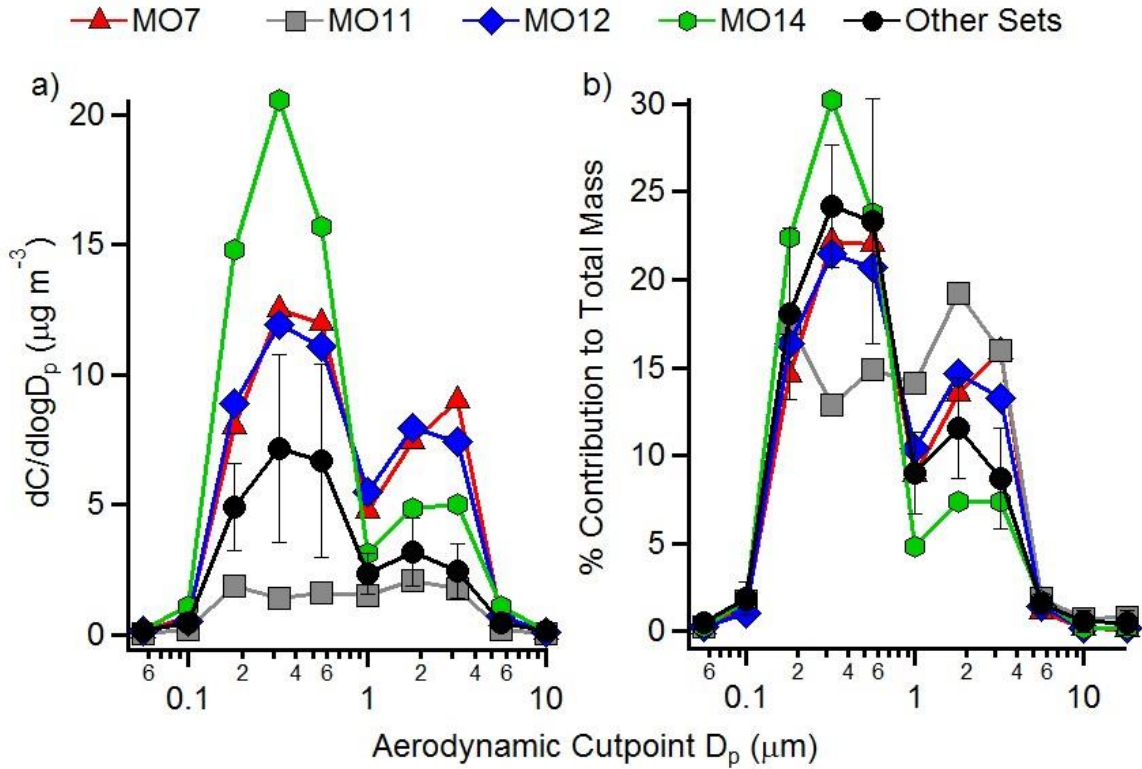


1250
 1251
 1252
 1253
 1254
 1255
 1256

Figure 3. CALIOP Vertical Feature Mask (VFM) for overpasses during or following MO7, MO12, and MO14. For the CALIPSO satellite overpass tracks, the dashed lines correspond to the nighttime profiles and solid lines are for daytime. Note that nighttime overpasses correspond to early morning times before sunrise for the listed days and daytime overpasses occurred during early afternoon.

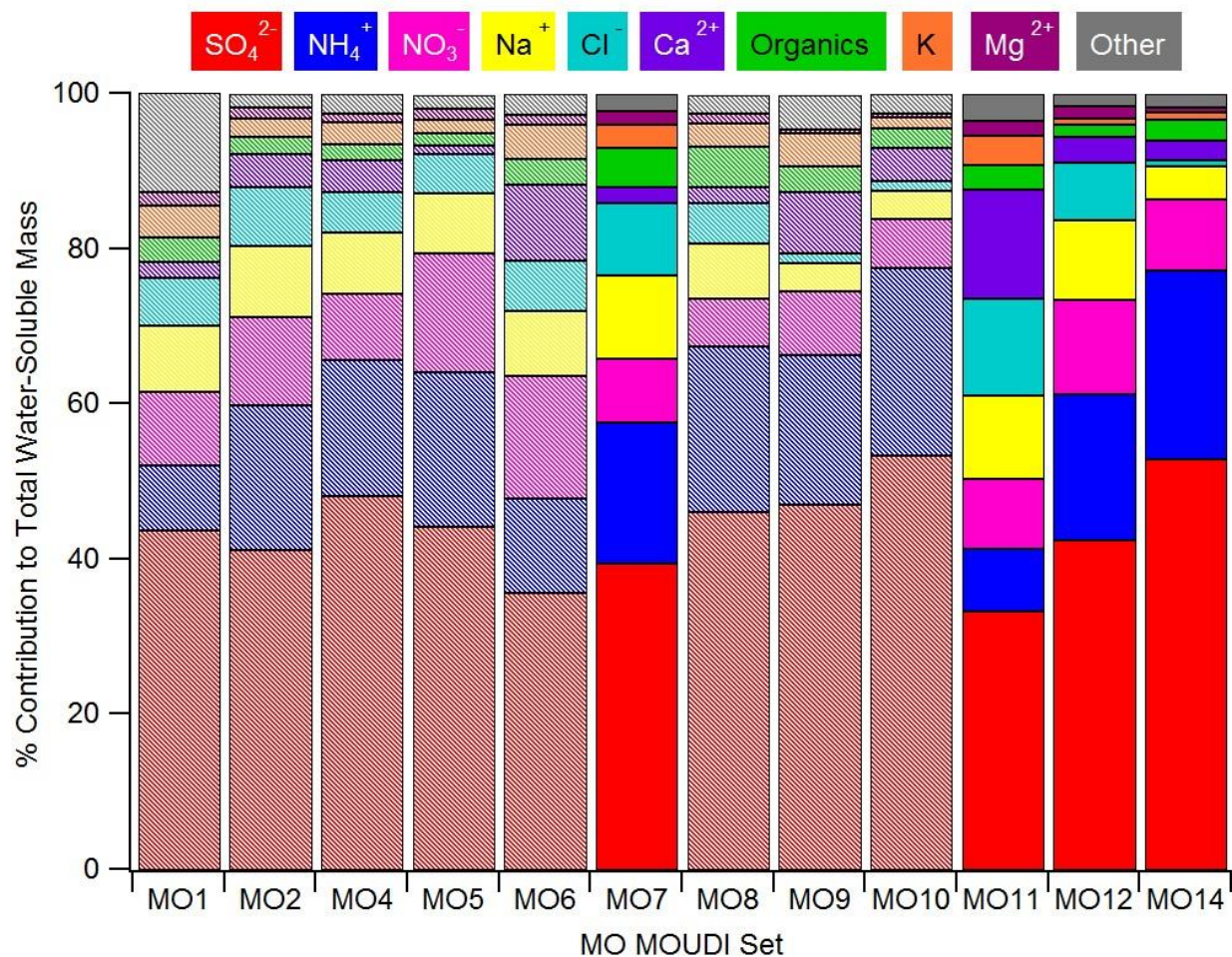


1257
 1258 **Figure 4.** NAAPS model snapshots corresponding to conditions at the stop time of sample sets a)
 1259 MO7, b) MO11, and c) MO12 and d) 3 h after the sample stop time for MO14. The top row of
 1260 figures is anthropogenic and biogenic fine aerosol (ABF) surface concentration ($\mu\text{g m}^{-3}$), while
 1261 the bottom row is biomass burning smoke surface concentration ($\mu\text{g m}^{-3}$).

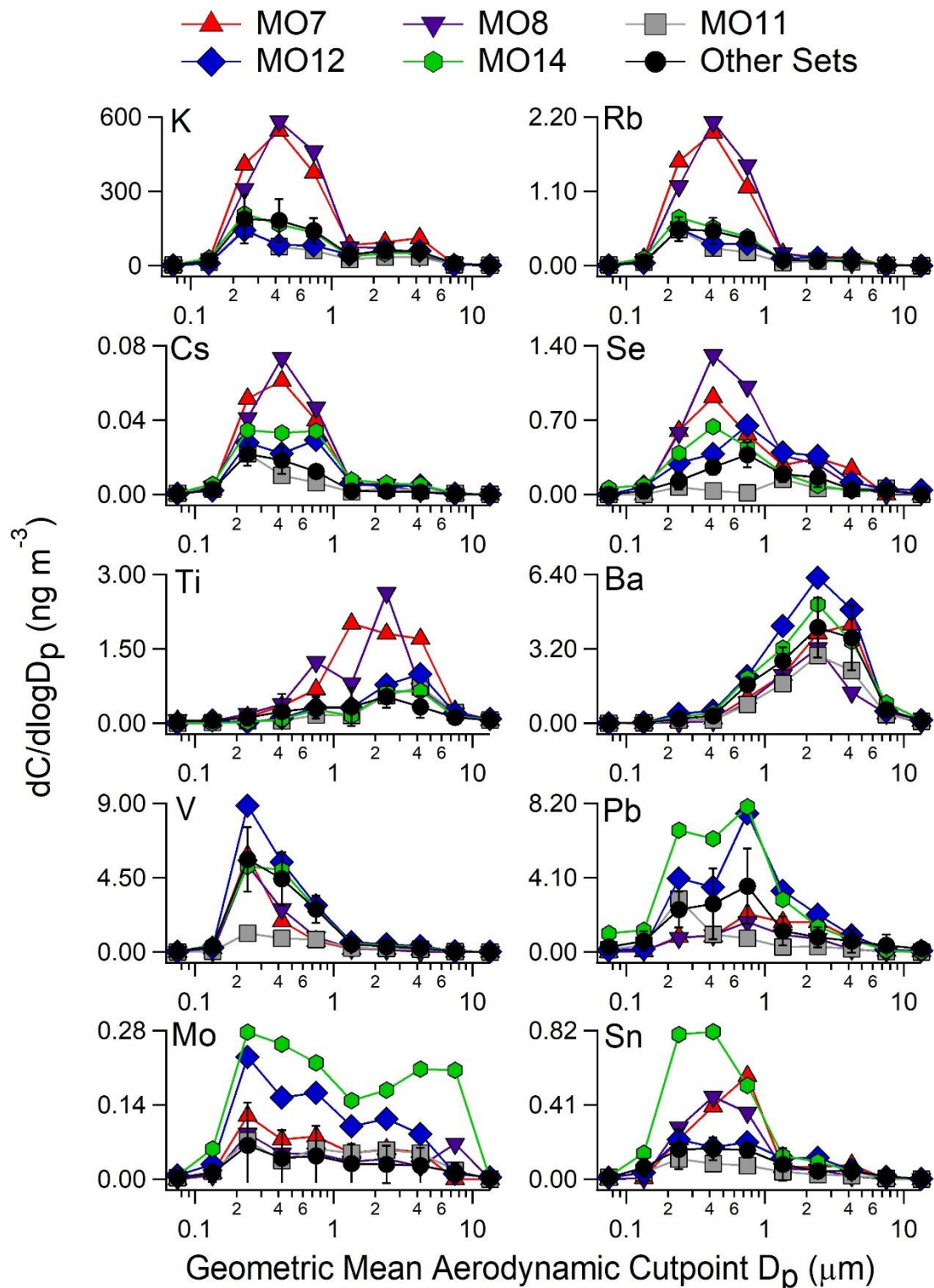


1262
 1263
 1264
 1265
 1266
 1267
 1268

Figure 5. a) Mass size distributions for total water-soluble mass ($C =$ sum of mass concentrations for water-soluble species) and b) percent contribution of each size range to the total water-soluble mass for the three MOUDI sets with the highest aerosol mass concentrations (MO7, MO12, and MO14), the set with the lowest concentration (MO11), and the average (\pm one standard deviation error bars) for the remaining eight sets.

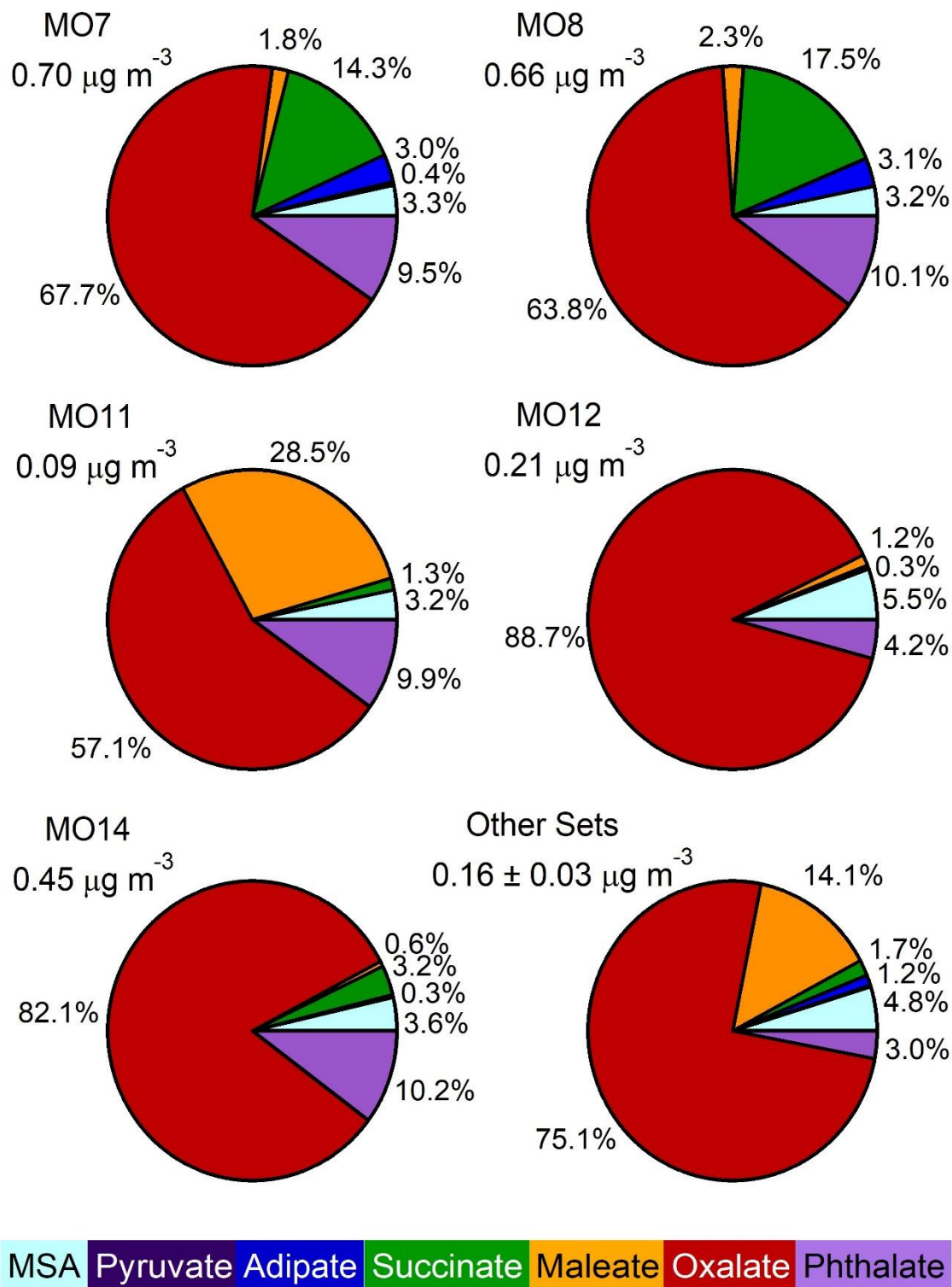


1269
 1270 **Figure 6.** Percent contribution of various species to the total water-soluble mass concentration
 1271 for each of the 12 sample sets. The sample sets with the three highest aerosol concentrations
 1272 (MO7, MO12, and MO14) and the lowest aerosol concentration (MO11) are shown as solid bars
 1273 while all other sample sets are stripes. The “organics” category contains the sum of
 1274 methanesulfonate (MSA), pyruvate, adipate, succinate, maleate, oxalate, and phthalate.



1275
 1276
 1277
 1278
 1279

Figure 7. Selected elements that showed elevated concentrations during at least one of the highest aerosol events (MO7, MO8, MO12, or MO14). The concentrations from the lowest aerosol event (MO11) are also shown. The “other sets” category displays the average (\pm one standard deviation) for the remaining seven sets.



1280
1281
1282
1283
1284
1285

Figure 8. Pie charts showing the fraction of species contributing to the measured water-soluble organic aerosol. Below each pie chart title is the sum of the water-soluble organic species measured, with the “other sets” chart showing the average \pm one standard deviation for the remaining sets. Acronyms: Methanesulfonate (MSA)